UiT The Arctic University of Norway

Department of Electrical Engineering

Roach Infestation Optimization MPPT Algorithm of PV Systems for Adaptive to Fast Changing Irradiation and Partial Shading Conditions

Ntiakoh Kakra Nicholas

Master Thesis Electrical Engineering, ELE-3900, May 2021

<table>
<tr><td>Title:

Roach Infestation Optimization MPPT Algorithm of PV Systems for Adaptive to Fast Changing Irradiation and Partial Shading Conditions</td><td>Date:

May 15, 2021</td></tr>
<tr><td rowspan="2">Subject Name:
Master Thesis – M-EL</td><td>Classification:
Open</td></tr>
<tr><td>No. of pages: 55</td></tr>
<tr><td>Faculty:
Faculty of Engineering Science and Technology</td><td>No. of attachments: 1

Subject Code: ELE-3900</td></tr>
<tr><td colspan="2">Master Program:
Electrical Engineering</td></tr>
<tr><td colspan="2">Supervisor:
Dr. Chittaranjan Pradhan</td></tr>
<tr><td colspan="2">Keywords:
Boost converter, Non-isolated DC-DC converter, Maximum power point tracking (MPPT), Partial shading condition (PCS), Population-based Optimization, Roach Infestation Optimization (RIO), Solar Photovoltaic (PV)</td></tr>
</table>

ACKNOWLEDGMENT

My profound gratitude goes to ALMIGHTY God for his protection and guidance throughout my course of study.

I would like to show my sincere gratitude to my supervisor: Dr. Chittaranjan Pradhan for his guidance, support, patience, motivation, assistance and technical guidance throughout the duration of this thesis work. I convey my gratitude to Dr. Trond Østrem, Dr. Pawan Sharma, Dr. Bjarte Hoff, Mr. Arild Steen, Head of the Department in the Electrical Engineering and other members for their help and motivation through my period of M.Sc. study.

I will remain ever grateful to the Norwegian Government through UDI for allowing me to improve my knowledge in a world-class University-UiT The Arctic University of Norway, it is a dream come through.

I will also say a big thank you to my family for the support throughout my entire life and for their well wishes.

I will also show my gratitude to my friends for always pushing me to give it my best. Thank you very much for the love and care.

Last but not the least, I am very grateful to the Arctic Centre for Sustainable Energy (ARC), UiT The Arctic University of Norway, Norway for providing an environment to do this work. This work was supported in part by the ARC, Norway under Grant 310059.

Nicholas Kakra Ntiakoh

ABSTRACT

Of all the renewable energy sources, solar photovoltaic (PV) power is considered to be a popular source owing to several advantages such as its free availability, absence of rotating parts, integration to building such as roof tops and less maintenance cost. The nonlinear current–voltage (*I–V*) characteristics and power generated from a PV array primarily depends on solar insolation/irradiation and panel temperature. The power output depends on the accuracy with which the nonlinear power–voltage (*P–V*) characteristics curve is traced by the maximum power point tracking (MPPT) controller. A DC-DC converter is commonly used in PV systems as an interface between the PV panel and the load, allowing the follow-up of the maximum power point (MPP). The objective of an efficient MPPT controller is to meet the following characteristics such as accuracy, robustness and faster tracking speed under partial shading conditions (PSCs) and climatic variations. To realize these objectives, numerous traditional techniques to artificial intelligence and bio-inspired techniques/algorithms have been recommended. Each technique has its own advantage and disadvantage. In view of that, in this thesis, a bio-inspired roach infestation optimization (RIO) algorithm is proposed to extract the maximum power from the PV system (PVS). In addition, the mathematical formulations and operation of the boost converter is investigated.

To validate the effectiveness of the proposed RIO MPPT algorithm, MATLAB/Simulink simulations are carried out under varying environmental conditions, for example step changes in solar irradiance, and partial shading of the PV array. The obtained results are examined and compared with the particle swam optimization (PSO). The results demonstrated that the RIO MPPT performs remarkably in tracking with high accuracy as PSO based MPPT.

Abbreviation

ABC	Artificial bee colony algorithm
AC	Alternating Current
ACO	Ant Colony Optimization
AM	Actual Measurement
ANN	Artificial Neural Network
CCM	Continuous Conduction Mode
CCP	Common Coupling Point
CF	Curve Fitting method
CS	Current Scanning method
CVT	Constant Voltage Tracking
DC	Direct Current
DCM	Discontinuous Conduction Mode
DE	Differential Evolution
DG	Distributed Generation
DS	Dominance Square
DSP	Digital Signal Processor
EMI	Electro-Magnetic Interference
FA	Firefly Algorithm
FLC	Fuzzy Logic Controller
FLS	Fibonacci Linear Search algorithm
FPGA	Field Programmable Gate Array
FWA	Firework algorithm
GMPP	Global Maximum Power Point
GWO	Grey Wolf Optimization

HC	Hill Climbing
HM	Hysteresis Modulator
IC	Incremental Conductance
IGBT	Insulated Gate Bipolar Transistor
IPSO	Improved PSO
LMPP	Local Maximum Power Point
LT	Look-up Table method
MATLAB	MATrix LABoratory
MH	Metaheuristic
MMP	Maximum Power Point
MMPT	Maximum Power Point Tracking
MOSFET	Metal-Oxide Field Effect Transistors
MSSA	Memetic Salp Swarm Algorithm
NN	Neural Network Controller
NPU	New Pheromone Updating
OD-PSO	Overall Distribution-PSO
OVT	Open-circuit Voltage Tracking
P&O	Perturbation and Observation
PAC	Photovoltaic Array Combination
PC	Parasitic Capacitance
PF	Power Feedback
PMW	Pulse Width Modulation
PSC	Partial Shading Condition
PSCs	Partial Shading Conditions
PSO	Particle Swarm Optimization

PV	Photovoltaic
PVS	Photovoltaic System
RBF	Radial Basis Function
RCC	Ripple Correlation Control
RCGA	Real-Coded Improved GA
RES	Renewable Energy Source
RPV	Re-configurable PV
SCT	Short-circuit Current Tracking
SMC	Sliding-Mode Control
SS	Simple Series
SSA	Salp Swarm Algorithm
SSM	Segmentation Search Method
VO-MPPT	Voltage-oriented MPPT

Nomenclature

A	Ampere in unit

C	Coulomb in unit
D	Duty cycle or duty ratio of the DC-DC converter
f_s	Switching frequency (Hz)
k	Boltzmann's constant (joule (J)/kelvin (K)
n	Diode ideality factor (1 for an ideal diode)
q	Elementary charge of the PV cell (C)
s	Second in unit
T	Pulse width or time-period of the DC-DC converter (s)
V	Voltage in unit
D_d	Diode of the PV cell
I_d	Diode current of the PV cell (A),
I_{rs}	Reverse saturation current (A)
I_{ph}	Light-generated current in the PV cell (A)
I_{pv}	Output PV cell current (A)
I_{sc}	Short-circuit current (A)
I_{sh}	Shunt current of the PV cell (A)
R_s	Series resistance of the PV cell (Ω).
R_{sh}	Shunt resistor of the PV cell (Ω)
V_{oc}	Open-circuit voltage of the PV cell (V)
T_0	PV cell absolute temperature (^{0}K)
T_r	PV cell reference temperature (^{0}K)
D_i	Diode of the DC-DC converter
C	Capacitor of the DC-DC converter
L	Inductor of the DC-DC converter
L_{min}	Minimum inductance of the boost converter

R	Load resistor of the DC-DC converter
S_w	Switching MOSFET
V_{in}	Input voltage of the DC-DC converter
I_o	Output current of the DC-DC converter
V_o	Output voltage of the DC-DC converter
c_1	Acceleration constants in PSO
c_2	Social parameter in PSO
r_1 and r_2	Random numbers for PSO
w	Weight parameter in PSO
v^l_i	Velocity of i^{th} particle/agent for l^{th} iteration
x^l_i	Position or location of i^{th} particle/agent for l^{th} iteration
C_o and C_{max}	Constants in RIO
R_1	Vector of uniform random number in RIO
p_k	Darkest known location for the individual cockroach agent
C_o and C_{max}	Constants in RIO
g^{best}	Best global position of the particle
P^{best}	Best local position of particle
G_p	Global peak power of the PV system
I_{pv}^{max}	Current at MPP of the PV
P_{pv}^{max}	Power at MPP of the PV
V_{pv}^{max}	Voltage at MPP of the PV

Table of Contents

List of figures

Table of Figures

1 Introduction

Providing an affordable and reliable electricity supply has become an important requirement for modern society. According to International Energy Agency (IEA) of Organization for Economic Cooperation and Development, global electricity consumption is projected to be nearly double between 2015 and 2040, growing at an annual rate of 2.4%. This will rise by 60% between 2015 and 2040, accounting for 55% of the world's energy demand growth [1]. Consequently, in the World scenario, the projected electricity generation by different sources to increase rapidly as shown in **Figure 1.1 [1].** The projected total global electricity generation rises by more than 58% between 2015 and 2040.

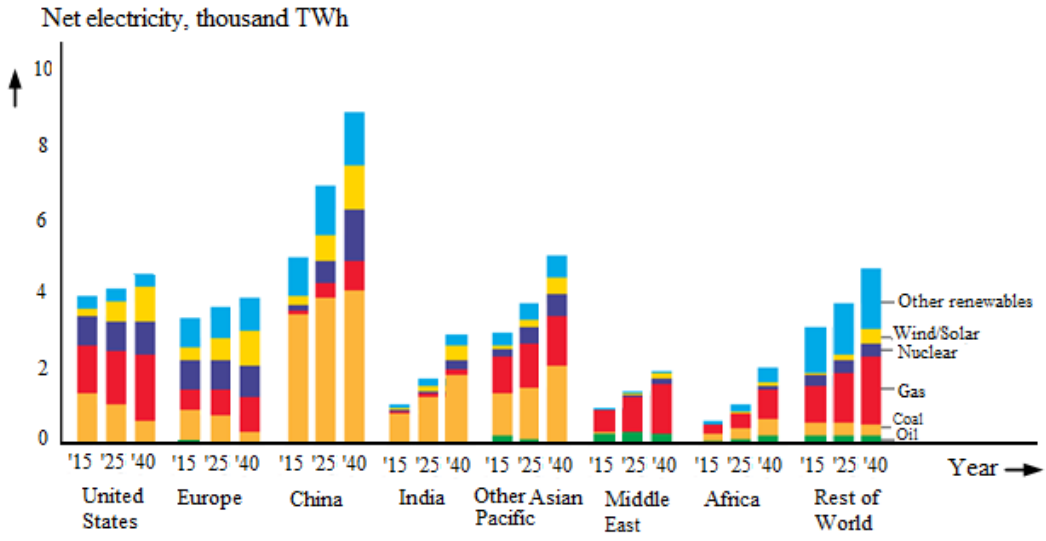

Figure 1-1:*Projected global electricity generation by region in World scenario [1]*

The use of non-renewable energy sources such as oil, coal, and natural gas for the production of electricity produces harmful emissions that affect the environment and cause global warming. The urgent necessity to protect this planet has called for cleaner sources of energy, of which solar power plays a significant role. Solar is a pollution-free source of energy, and it is abundantly available. This energy is harnessed through a photovoltaic cell with other technologies to provide heat, light, electricity for domestic use and industrial applications.

The global growth of solar PV capacity has been increasing consistently since 2000. Between 2000 and 2019, numbers grew by 632.4 gigawatts. In 2019, solar PV capacity reached 633.7 gigawatts globally, with 116.9 gigawatts installed that year [2]. **Figure 1.2** shows the actual cumulative capacity in gigawatts by select countries as of 2019.

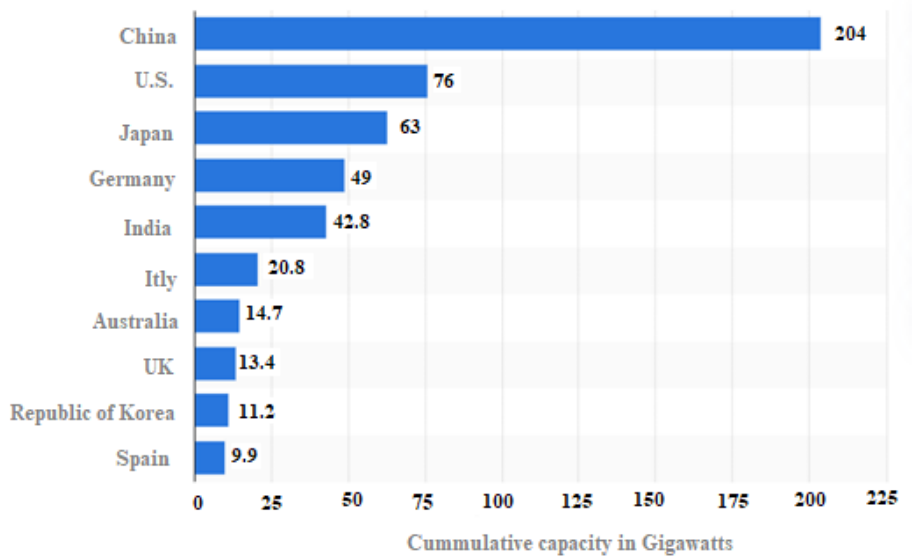

Figure 1-2: *Global cumulative solar PV capacity by select country 2019 [2]*

In Norway, 98 per cent of electricity production comes from renewable sources putting the country in an unparalleled position in Europe and the global perspective. Production of electricity in the country is mainly dependent on hydropower, but thermal and wind energies also contribute to Norwegian electricity production [3]. **Figure 1.3** shows the energy consumption by source in Norway from 1965 to 2019.

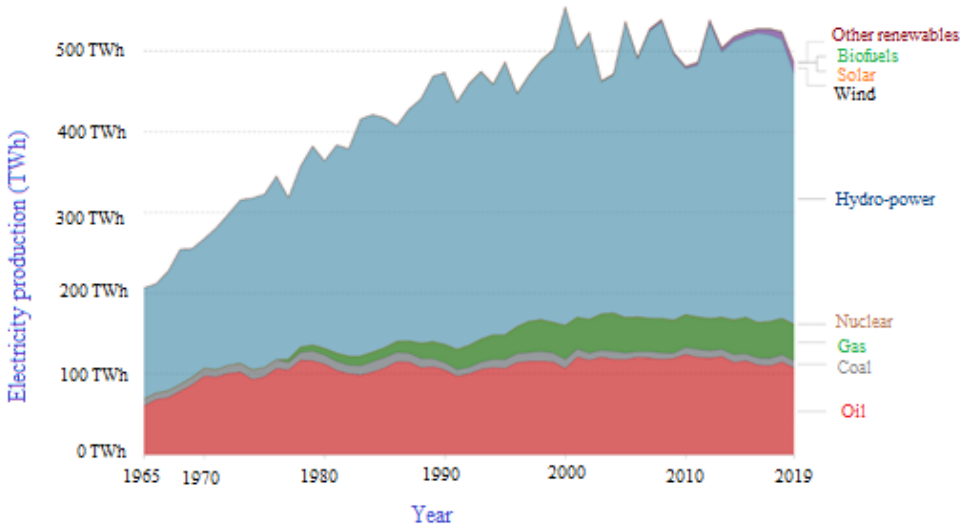

Figure 1-3: *Energy consumption by source, Norway [4]*

At the beginning of 2021, the total capacity of solar power installed in Norway was 160 MW. Statistics showed that about 90% of the installed capacity, corresponding to around 7000 photovoltaic systems, was linked to the power grid. Statistics also show that though 85% of the

photovoltaic systems are plants of less than 15 kW, these account for only a third of the production capacity.

In 2020, approximately 40 MW of solar power was installed in Norway, corresponding to 350 solar panels installed each day in 2020. This increased the power capacity by 40% during the year. It became higher in 2019 when the capacity increase was estimated at 50 MW [5]. The figure below displays the bar chart of solar power installed in Norway from 2004 to 2020.

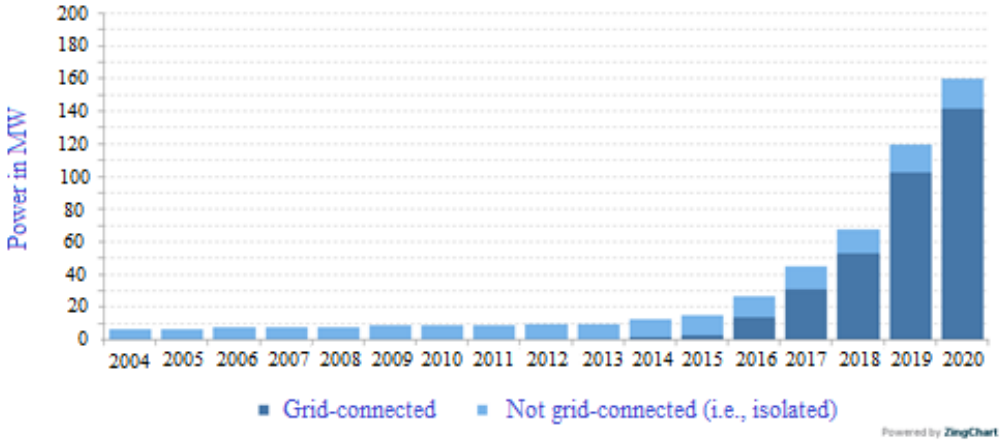

Figure 1-4: *Development in installed capacity for solar power in Norway [5]*

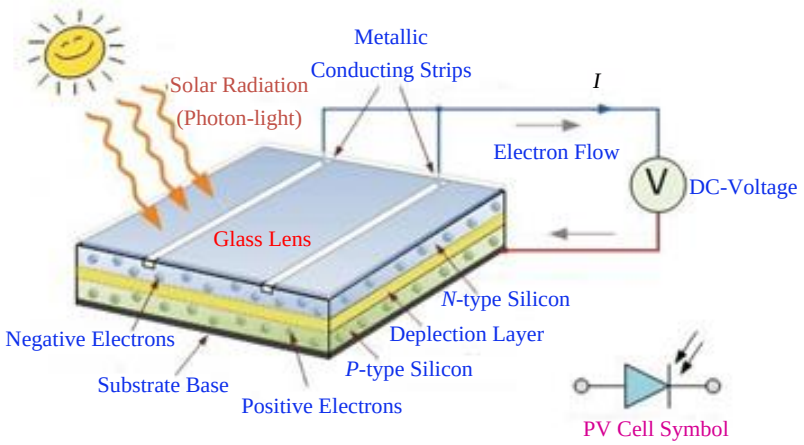

Figure 1-5*: Photovoltaic solar cell construction [6]*

Photovoltaics (PVs) is converting light (from the sun) into electricity by the use of semiconducting materials that exhibit the photovoltaic effect. A PV system employs solar modules, which comprise several solar cells, generating electrical energy or power [7]. **Figure 1.5** shows the PV solar cell construction. Despite the recent technological enhancement in PV utilization characteristics, such as reducing cost and improving efficiency, the low energy conversion efficiency of PV systems remains a significant drawback to the utilization of PV power.

One other major issue with PV power generation is the reliance on environmental factors, such as solar irradiance and ambient temperature. Since the cost involved in PV power generation is high and to make to most profit on investment, it is very important to extract most of the available solar energy through the panels. Therefore, the control unit of the PV system must be compelled through a better MPPT technique to extract the maximum power from the installed PV arrays by providing a suitable duty ratio to control the DC-DC converter embedded in the system. Taking into account all affecting factors of the PV, boosting the MPPT efficacy is a low-cost method of improving the performance of the PV system [8].

1.1 Basic components and configuration of PV

A cell in the PV panel is a semi-conductive material that converts the light from the sun into electricity. A PV module is several PV cells linked in series. Connection of modules in series or parallel forms an array. A string is a series-connected set of solar cells or modules. **Figure 1.6** shows the PV cell, module, string and array.

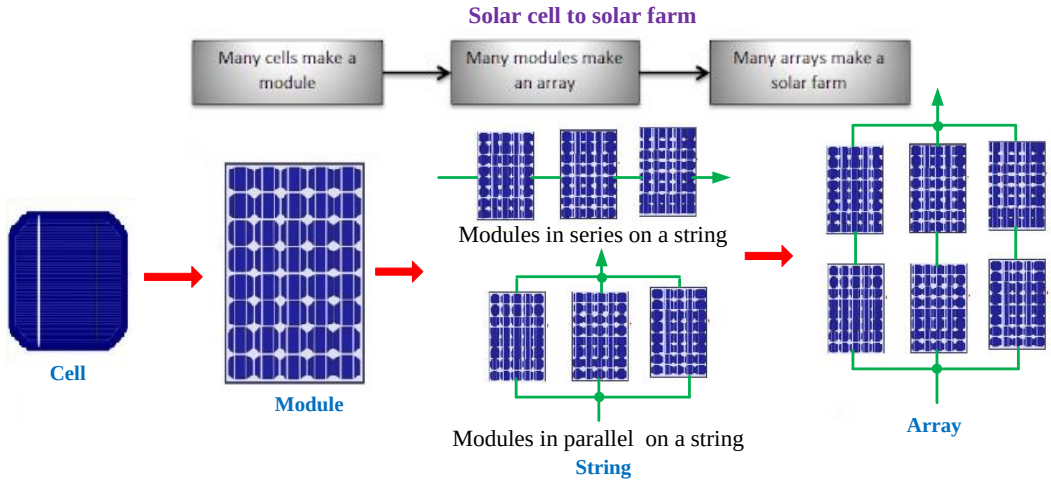

Figure 1-6: *Cell, module, panel, and array*

The output voltage of a typical PV cell is around 0.6V at 25°C (normally around 0.58V) irrespective of how big they are [9]. The panels are connected in series and or parallel to gain the voltage and or current required. Series and parallel configurations are the basic configurations used; therefore, other configurations are derived [10]. Other topologies of PV configuration are the series-parallel (SP), total-cross-tied (TCT), bridge-linked (BL), etc.

Series–parallel (SP): in this configuration, all the solar modules are initially connected in series, then these series connections are then combined in parallel. The shading effect on one of the modules of the SP string causes losses that affect all the modules in that string. One

advantage is, when the shading effect occurs, only one string of the SP array is affected, while in series, the entire array is affected [11].

Total-Cross-Tied (TCT): this is derived from SP configuration by connecting crossties across each module's row. The voltage across each row is the same, and the sum of current across each column is the same in this configuration [11].

The Bridge Linked (BL): Aims to reduce the number of connections between adjacent strings of modules by about half compared to the topology (TCT), which significantly reduced the amount and wiring length of the PV array [11]. **Figure 1.7** shows the solar configurations explained above.

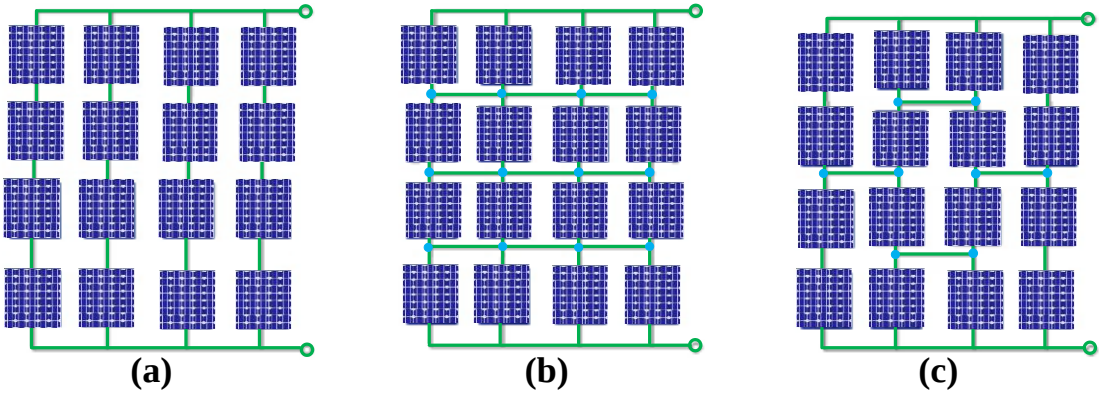

Figure 1-7: (a). *Series-parallel (SP),* ***(b).*** *Total-cross-tied (TCT),* ***(c).*** *Bridge–linked [12]*

1.2 PV Modelling and Characteristic

To establish the behaviour of a solar cell electronically, an equivalent model is made based on basic electrical components whose behaviour is well known. It is modelled by a current source in parallel with a diode, a shunt resistance and a series resistance component [13]. The equivalent model of a solar cell is shown in **Figure 1.8.**

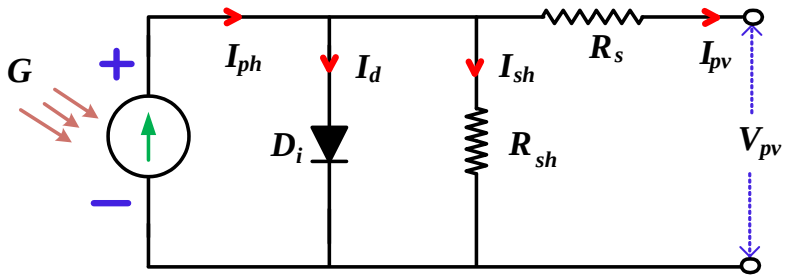

Figure 1-8: *Equivalent model of a solar cell*

In **Figure 1.8**, R_s and R_{sh} are the intrinsic series and shunt resistor of the PV cell (Ω), respectively. I_{sh} is the current through R_{sh}. D_i is the intrinsic Diode. I_d is diode current (A), I_{sh} is

shunt current (A), I_{ph} is the light-generated current in the cell (A). V_{pv} and I_{pv} are the PV output voltage and current, respectively. G is the solar irradiation.

1.2.1 Characteristic equation

From **Figure 1.8**, the current generated by the solar cell is equivalent to that produced by the current source minus that which flows through the diode and the shunt resistor. This established by equation (1.1) by Kirchhoff's current law [14].

$$I_{pv} = I_{ph} - I_d - I_{sh} \tag{1.1}$$

The current through these elements can be given by the voltages across them:

$$V_d = V_{pv} + R_s I_{pv} \tag{1.2}$$

Where, V_d is the voltage across the diode (V).

The PV cell is quantified by current-voltage characteristic operation as follows [14]:

$$I_{pv} = n_p I_{ph} - n_p I_p \left[\exp\left(\frac{q(V_{pv} + I_{pv} R_s)}{AKT n_s} \right) - 1 \right] - \left(\frac{V_{pv} + I_{pv} R_s}{R_{sh}} \right) \tag{1.3}$$

with $$I_p = I_{rs} \left[\frac{T}{T_r} \right]^3 \exp\left(\frac{qV_{oc}}{AK} \left[\frac{1}{T_r} - \frac{1}{T} \right] \right), \quad I_{ph} = I_{sc} + \left[K(T_0 - T_r) \right] \frac{G}{1000}$$

where, n_s and n_p are the number of cells connected in series and parallel, q is the electron charge (C), K is Boltzmann's constant (J/K), A is the *p-n* junction's idealistic factor, T is the cell's absolute temperature (^{0}K), T_r is the cell reference temperature (^{0}K), I_{ph} is the cell's photocurrent (it depends on the solar irradiance and temperature), I_{rs} is the cell's reverse saturation current, I_{sc} is the short-circuit current of the PV cell, V_{oc} is the open-circuit voltage of the PV cell *and* G is the solar irradiance.

1.3 Effect of Variation of Temperature and Irradiation

The *P-V* and *I-V* curves of a solar cell heavily depend on the solar irradiation level and temperature. Solar irradiation and temperature as a result of environmental conditions keep on changing throughout the day. Control mechanisms are put in place to track the changes to alter the working of the solar cell to meet the required output. The open-circuit voltage increases

with an increase in solar irradiation. This is because, when more sunlight incidents on the solar cell, the electrons gain higher excitation energy, thereby increasing the electron mobility, and thus, more power is generated. **Figure 1.9** shows the effect of the variation of solar irradiation on the PV cell. It is shown that as the irradiation increases, the power and current of the solar PV increases as the solar irradiation increases.

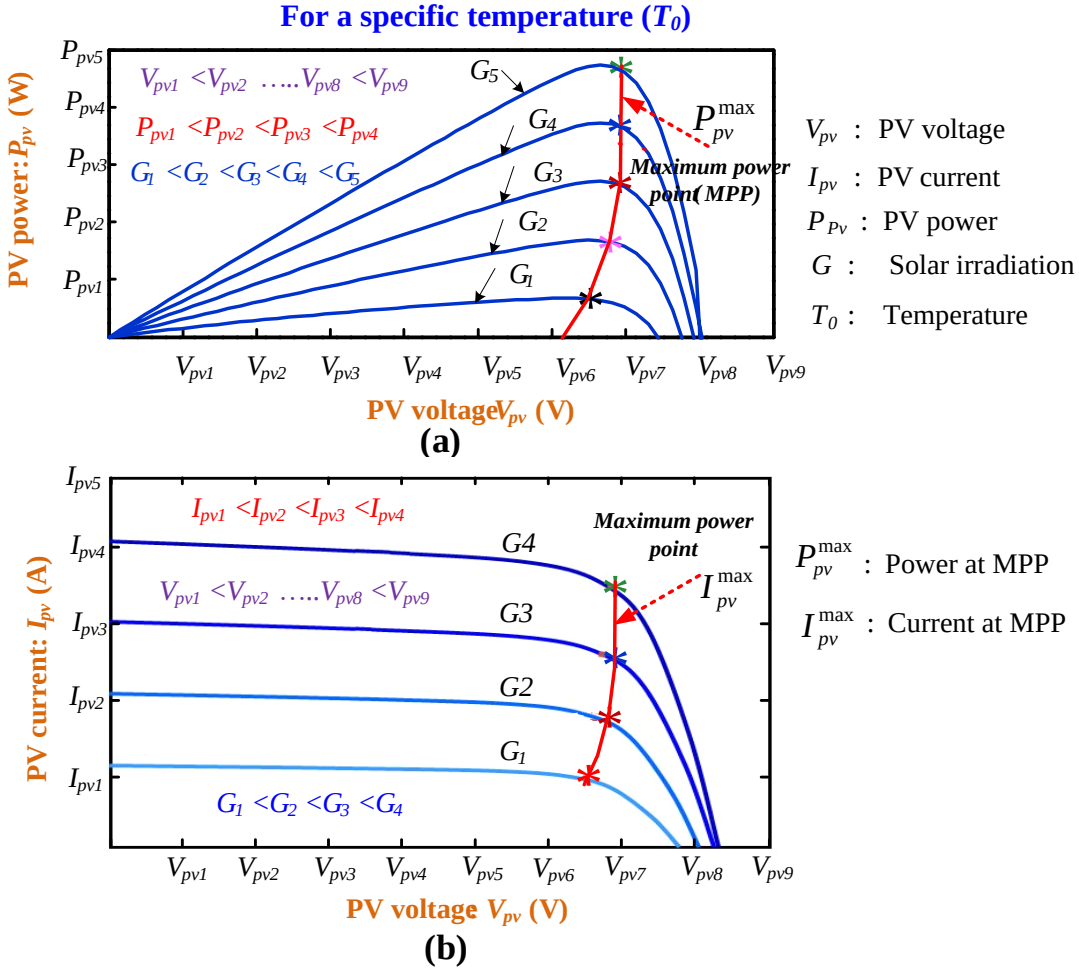

***Figure 1-9**: **(a).** P-V curve, and **(b).** I-V curve with respect to variations of solar irradiation*

On the contrary, an increase in temperature negatively affects the power generation capability of the solar cell. A temperature rise corresponds to a reduction in the open-circuit voltage. This causes an increase in the bandgap of the material, and thus more energy is needed to cross this barrier causing the efficiency of the solar cell to reduce [15]. **Figure 1.10** shows that as the temperature increases, the solar power of the PV decreases and vice versa.

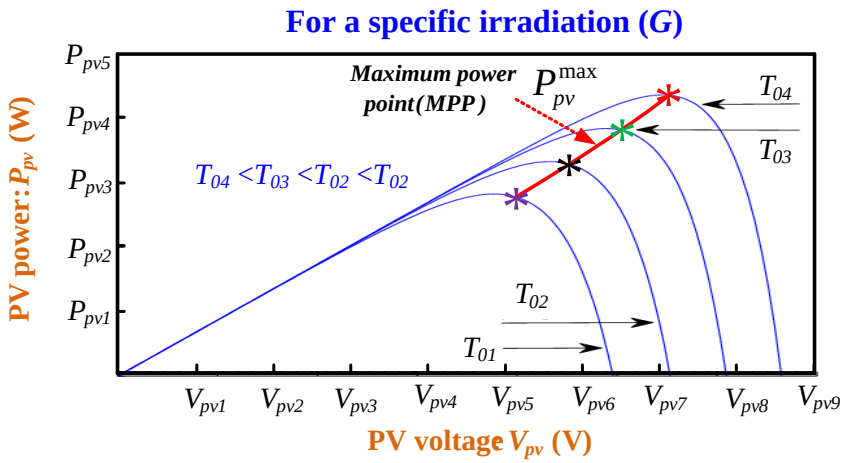

***Figure 1-10**: P-V curve with respect to the variations of temperature*

1.3.1 Partial Shading Condition

The performance or the output of a photovoltaic (PV) array is highly affected by temperature, solar insolation, shading, and array configuration. Usually, the PV arrays get shadowed entirely or fractionally by the passing clouds, neighbouring buildings, trees, etc. In this situation, the current (power) generated by other cells cannot pass through the shaded cells and is given out in heat. **Figure 1.11(a)** shows that the shaded cells are forced to operate with a reverse bias voltage to provide the same current as that of the unshaded cells. The current flowing through the entire module in a series configuration is constant. However, the resulting reverse power polarity absorbs power and reduces the power output of the shaded PV system. Continuously operating the shaded cells in reverse bias voltage may cause hot spots and an open-circuit in the entire PV array [16].

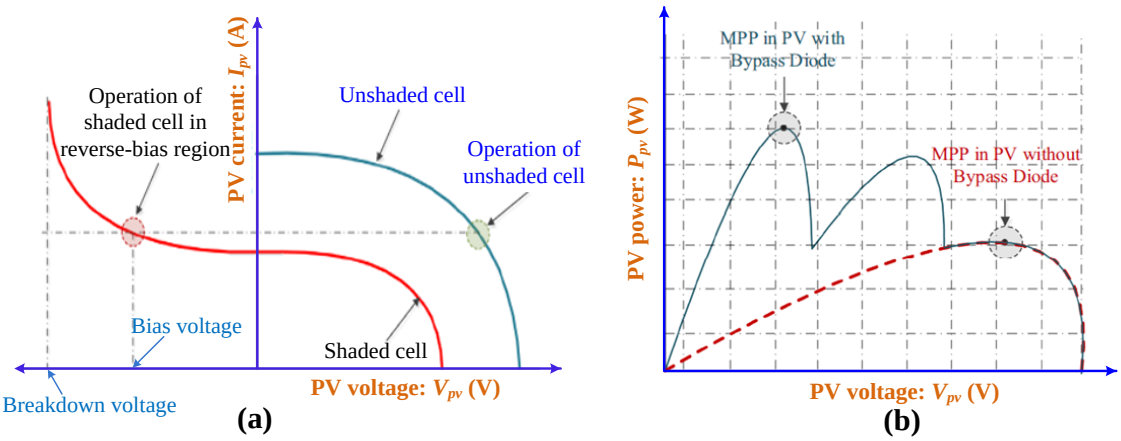

***Figure 1-11: (a).** P–V curve of a PV array under PSCs, **(b).** I-V graph of PV cells in a reverse bias region [16]*

Figure 1.11(a) shows how the solar cell works under both shaded and unshaded conditions and **Figure 1.11(b)** represents the PV graph of the PV cell with and without bypass diodes. It shows how MPP differs in the shaded PV array with and without bypass diodes. This results in power loss dramatically and can cause other serious problems such as hotspots which may melt the solar cells and eventually destroy the solar array [17]. To prevent this from happening, bypass diodes are used parallel with solar cells to limit the problems caused by partial shading. While the solar cell works, the diode works in reverse biased mode and has no role in system performance. When the paralleled cell with the diode gets shaded, the diode provides a current path for other cells and prevents the hotspots from happening. However, adding bypass diodes increases the complexity of the circuitry of the solar cell and creates multiple peaks in its current-voltage curve. This causes the PV system to exhibit extra difficulties when tracking the MPP because their *P-V* characteristics become complex and have multiple local maxima. **Figure 1.12(a)** shows the configuration of the PV array under PSC, **Figure 1.12(b)** the *P-V* curve for each sting under uniform and PSCs and **Figure 1.12(c)** is the resultant *P-V* plot under PSCs.

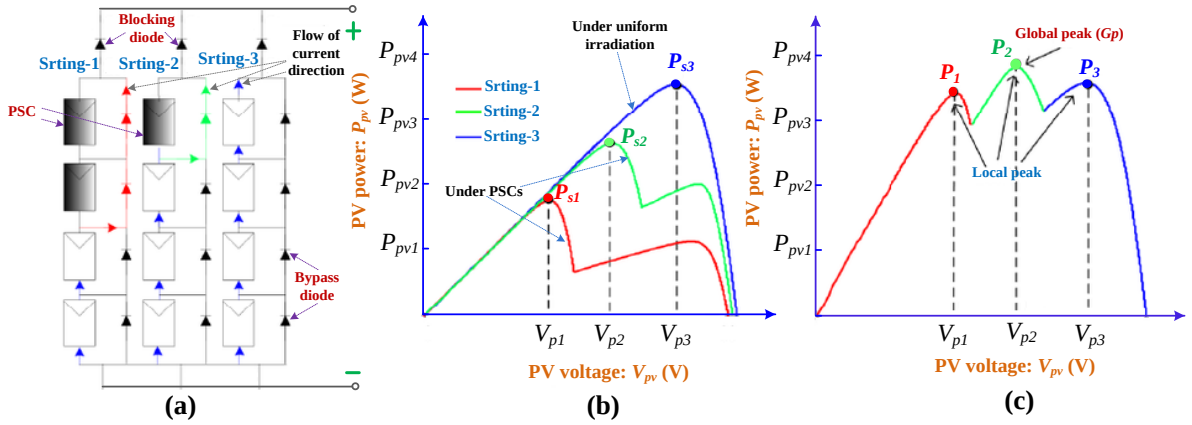

Figure 1-12: ***(a).*** *Configuration of the PV array system,* ***(b).*** *P–V curve for each string under PSC,* ***(c).*** *Resultant P–V curve under PSC*

1.4 Problem Statement

Photovoltaic (PV) technology has leading topic recently due to its harmless effect on the planet. Irradiation and temperature are the main factors that affect the performance of the PV system. However, when partial shading from surroundings occurs, irradiation reduces, affecting the generated power output. Since traditional MPPT techniques fail to track the maximum global power of the power-voltage (*P-V*) characteristic that arises due to this condition, a new tracking method needs to be developed to locate the global MPP of the system. This project aims at

proposing an MPPT algorithm to harness the optimum power from the solar panels under fast irradiation changing and PSCs.

1.5 Objectives

- Literature Review of PV based MPPT algorithms
- Literature Review of conventional DC-DC converter topologies
- Proposing an intelligent (soft computing) based MMPT algorithm for PV system
- Developing the simulation in MATLAB/Simulink platform
- Deployment of the Arduino or FPGA board (i.e., Hardware implementation) to validate the MPPT algorithm/control
- Based on this, a high gain transformerless converter topology could be further developed

1.6 Project Structure

This project is presented as follows. In the ***first Chapter***, an introduction or an overview is made to the research topic. The ***second Chapter*** introduces the literature review on some PV-based MPPT algorithms and DC-DC converter topologies. ***Chapter-three*** is the modelling of the DC-DC boost converter used. In ***Chapter-four***, RIO MPPT algorithm is proposed. ***Chapter-five*** discusses the simulation results obtained from the simulation. ***Chapter-six*** presents the conclusions. In this chapter, a conclusion is given on the work done, and possibilities for future work is proposed.

2 Literature review of MPPT algorithms and Conventional DC-DC Converters for PV Applications

2.1 Literature Review of PV based MPPT algorithms

In the past decades, solar energy has been one of the preferred conventional energy sources due to its low operation cost, nearly maintenance-free, and eco-friendly because it is one of the cleanest energy sources [18, 19]. The reliance on climatic changes and the high installation cost are the significant challenges of the PV system. Since PV cells are based on semiconductor materials, they show nonlinear power-voltage characteristics, which require a maximum power point tracking technology to increase power extraction under all conditions. The MPP is a distinctive point on the (*I*-*V*) or (*P*-*V*) plot at a given solar irradiance and temperature at which the PV system operates with optimal efficiency and produces its full output power. Since these climatic conditions vary continuously throughout the day, tracking the maximum power point from the PV is very challenging. To solve these issues, several MPPT techniques have been reported to improve the overall performance of the PV system [20-27]. Based on their search performance, application and mathematical formulation of the MPPT techniques are classified in three-methods as shown in **Figure 2.1**[28]

i. *Traditional MPPT methods:* The most commonly used traditional MPPT methods can be categorized into two types: the control methods based on parameter selection and the direct MPPT control technique based on sampled data. The most common traditional MPPT techniques are the Incremental conductance (IC) method [29, 30], perturb and observe (P&O) [31], and hill-climbing (HC) method [32]. These traditional methods are simple, easy implementation, and can track the MPP efficiently under normal conditions. However, they have a disadvantage as continuous oscillations occur around the MPP, causing significant power loss during a steady state. In addition, these methods are inefficient in managing the problem of PSCs due to the presence of multiple peaks in the *P*-*V* characteristics.

ii. *Intelligent control based MPPT:* These MPPT controls were invented to counteract the shortcomings of the traditional MPPT methods.

iii. *MPPT methods used for partial shading:* Various artificial intelligent MPPT techniques have been implemented to handle the shortcomings of the traditional MPPT methods in especially highly intermittent condition [33, 34]. These include fuzzy logic control (FLC), artificial neural network (ANN), firefly algorithm (FA), particle swarm optimization (PSO), ant

colony optimization (ACO), flower pollination algorithm (FPA), bat algorithm, grey wolf optimization (GWO) [35, 36] and many more. In [37] presented a technique called flower pollination algorithm (FPA) to mitigate PSC in building integrated PV power system (BIPVPS). The results demonstrated that proposed trackers had high accuracy and stability in tracking the global MPP in all the tested scenarios. Flower pollination activities can take place at all scales, both local and global. The switching probability or proximity probability can be effectively used to switch between the local and global.

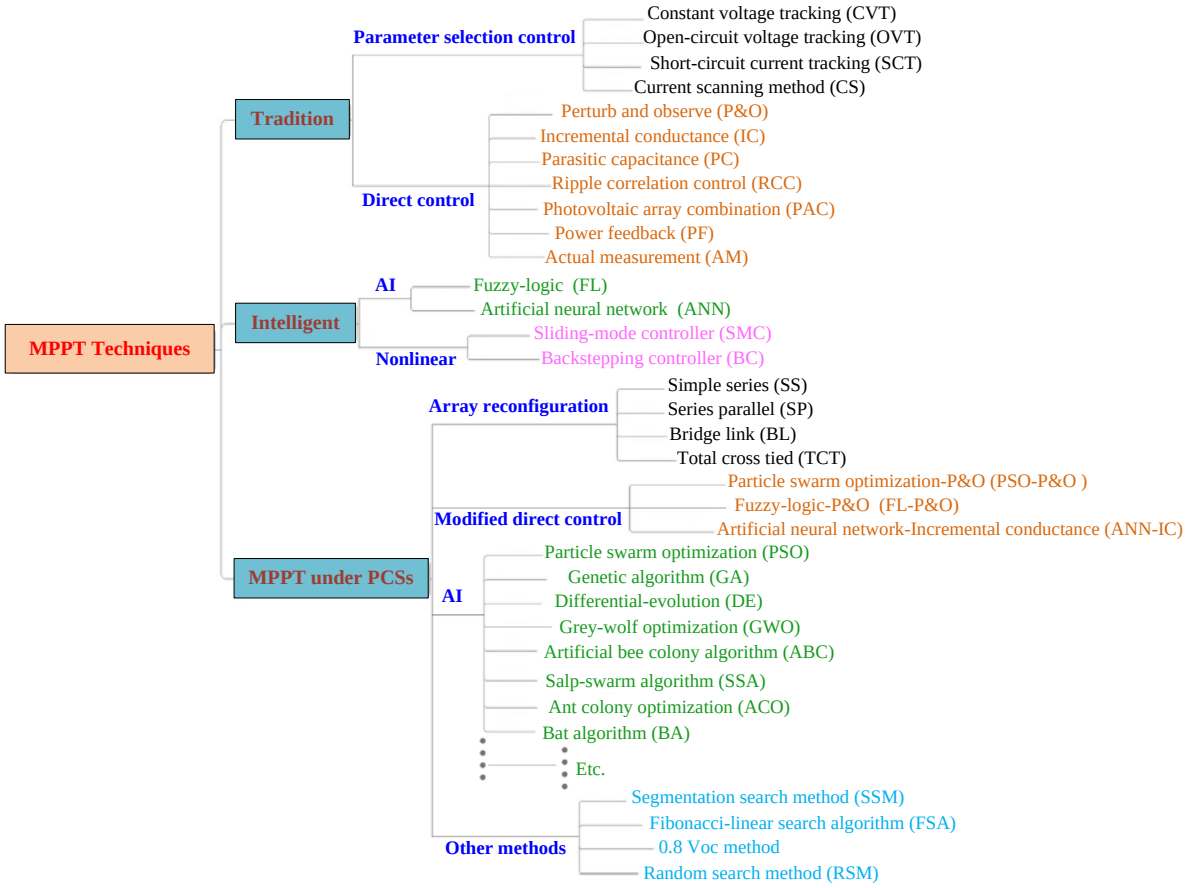

Figure 2-1: *Classification of some common MPPT control methods [28]*

Each algorithm can only be used at its best performance in an appropriate scenario and are generally not fitting for a wide range of applications. Hence, researchers suggest hybrid optimization techniques by combining two or more algorithms to improve the MPP tracking with less computational time. The simulated annealing with PSO (SA-PSOGWO-FL [38], PSO-P&O [39] and Jaya algorithm with differential evolution (Jaya-DE) [40] are such few examples. From this point of view, applying or designing a new MPPT algorithm in PV system for improving the search performance in real-time control problems is always welcome. By Seeing efficacy of the soft-computing based intelligent optimization algorithms, in this thesis, a bio-

inspired Roach Infestation Optimization (RIO) algorithm for tracking the maximum power from the PV is projected.

2.2 Literature Review of Conventional DC-DC Converter Topologies

Recently, the addition of electrical power to the grid through Renewable Energy Sources (RES) is on the rise. The distributed generation (DG) systems powered by sources like PV systems have also been adopted to meet the ever-increasing demand [41]. Power electronics is the use of solid-state electronics to control and conversion of electric power. Obtaining the maximum power from a panel is done with a DC-DC converter's aid [42]. These converters connect the RES to the grid. Power semiconductor switches like MOSFET or IGBT used in these converters operate when the appropriate pulse of suitable duty cycle is provided at the gate terminal to switch according to the desired output voltage. The DC-DC converters step down or step up the voltage from the generated voltage to the load [43]. Power electronics converters can be categorized into four groups based on their input and output. AC-DC (rectifier), DC-AC (inverter), DC-DC (DC-DC converter), and AC-AC (AC-AC converter)). These are further grouped into two: isolated and non-isolated converters, as shown in **Figure 2.2.**

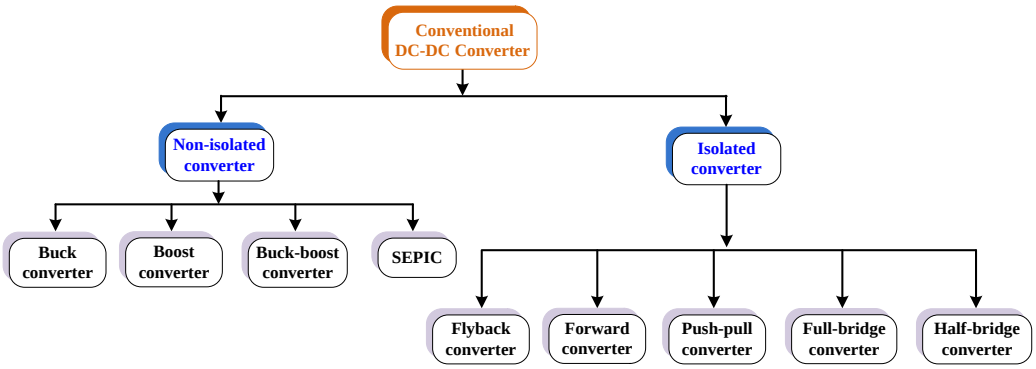

Figure 2-2: *Classification of DC-DC converter topologies*

Isolated converters separate the low voltage DC side from the high voltage side to prevent shock hazard, achieve high voltage conversion for voltage matching, and avoid large current or voltage rating semiconductor devices. High-frequency transformers are employed for such purposes. Its disadvantage is the use transformer core which makes it bulky and makes it more expensive. The non-isolated converters are simple in structure and are used primarily where galvanic insulation between source and load is not needed. The advantages of this group are low cost due to the use of fewer components and can gain high power density [44].

The following section presents an overview of the commonly used conventional buck, boost and buck boost converter topologies in solar PV. In this study, boost converter topology is used in the PV system.

2.2.1 Buck Converter

The DC-DC buck converter reduces the output voltage level when compared with the input voltage. The schematics of the buck converter is given in **Figure 2.3.** These are simple and efficient converters. They provide continuous output current and require a large capacitor to smoothen the discontinuous input current. They also need a higher gate side driver than the boost converter [45]. In **Figure 2.3**, V_{in} is the input voltage of the converter. V_0 are the output voltage. S_w is the switch (MOSFET), D_i is the diode, C is the capacitor, R is the load resistance and L is the inductor. The same symbols are used throughout the thesis to represent the variables/parameters.

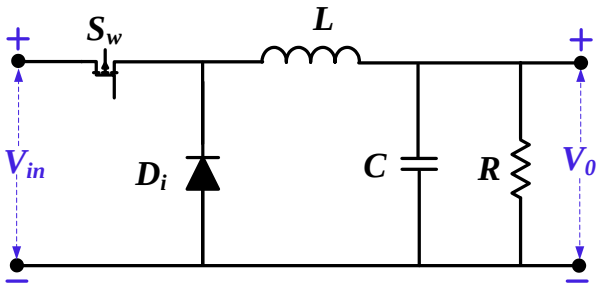

Figure 2-3: *DC-DC buck converter*

2.2.2 Boost Converter

It is a DC-to-DC converter that increases the input voltage to its output. The schematic of this converter is given in **Figure 2.4.** It has a continuous input current and a discontinuous output current. This converter provides a better dynamic response but a higher value of inductance than a buck converter is required. It needs a higher input side current, which may not always be available due to the shading of PV panels. The protection against the reverse current is provided naturally in these converters by the freewheeling diodes, but in a buck converter additional circuitry is required. The cost involved is cheaper than a buck converter due to a lower value input capacitor, lower current switch rating, and low side MOSFET driver requirement.

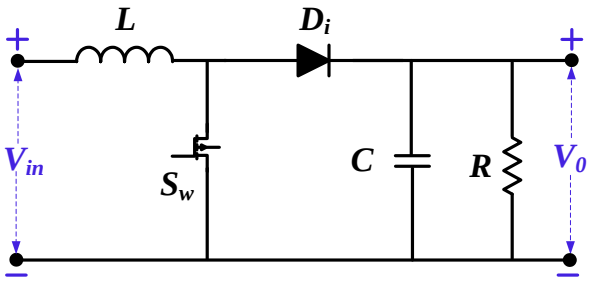

Figure 2-4: *Circuit diagram of a boost converter*

2.2.3 Buck-Boost Converter

The output voltage of this converter can be more or less than the input voltage. The schematics of the buck-boost converter is given in **Figure 2.5.** The magnitude of the output voltage depends on the duty cycle. They are also known as the step-up and step-down transformers and these names come from the traditional step up and step-down transformer.

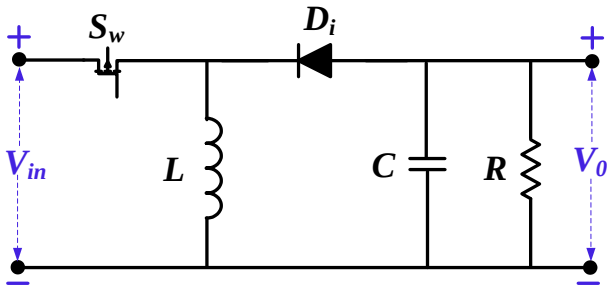

Figure 2.5*: Buck boost converter*

2.2.4 SEPIC Converter

Much attention has been given to the SEPIC topology recently because the output voltage maybe either higher or lower than the input voltage. It is a boost converter followed by an inverted buck-boost converter, making it similar to a traditional buck-boost converter. The schematics of the SEPIC converter is given in **Figure 2.6.** The output is also not inverted as is the case in a fly back or Cuk topology [46].

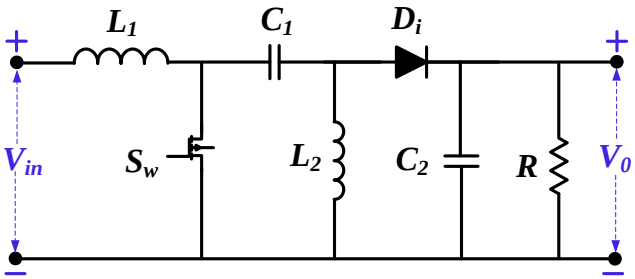

Figure 2-5: *SEPIC converter*

3 Boost Converter Design and Operation

Conventional energy sources such as photovoltaic (PV) require power electronic conditioning. The internal resistance of a solar PV panel alters with atmospheric conditions, but its load resistance remains unchanged. The MPPT algorithm integrated into a converter helps to achieve load matching and extracting maximum power from the PV panel. However, to ensure that the PV system is operating close to MPP, the DC-DC converter and the MPPT controller are placed between the load and PV modules [47].

The output of the PV cells is an unregulated low-level DC voltage that needs to be stepped up to a regulated higher level. For many applications, the DC-DC boost converter is proposed. This converter type has the advantages of being simple in structure, higher output voltage, and efficiency [48]. The converter's duty cycle is regulated at the appropriate output voltage of the system using the MPPT technique. The converter consists of a capacitor, an inductor a switch (MOSFET), and a diode. The switch is mainly controlled by the variable duty cycle from the MPPT algorithm at the operating frequency. There are two working modes of the boost converter based on the condition of the switch (ON or OFF).

3.1 Switching mode operations and State-space modeling of the Boost Converter

From **Figure 3.1**, when the converter's switch (S_w) is turned ON, D_i becomes reverse biased and doesn't conduct anymore whiles the inductor stores energy coming from the source. The inductor current (I_L) increases from the minimum value (I_{Lmin}) to the maximum value (I_{Lmax}) during this period. During this time, the load current is made continuous by the capacitor.

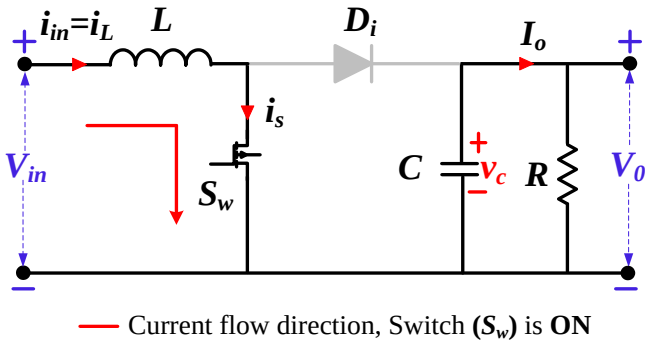

Figure 3-1: *Working mode when switch is ON*

From **Figure 3.2**, when the S_w is turned OFF, the I_L drops from the maximum value to the minimum value building up a negative voltage across the inductor (inductor polarity changes).

This negative voltage across the inductor puts the D_i in a forward-biased mode making it conduct. The energy stored in the inductor is then transferred to the load and capacitor through the diode. The main waveforms of the boost converter for ON/OFF operation mode are shown in **Figure 3.3.**

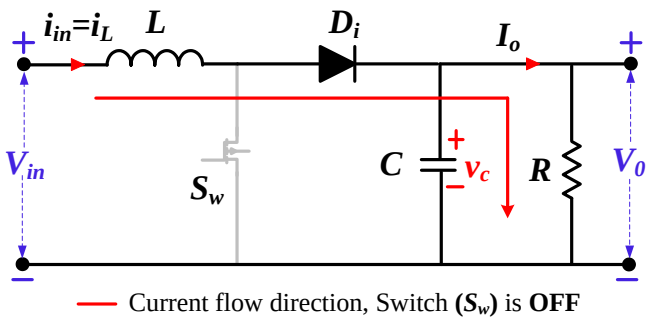

***Figure 3-2**: Working mode when switch is OFF*

The space-state model is based on the circuit shown in **Figures 3.1** and **3.2**. It is assumed that all components are ideal.

To apply averaging method for modelling, closed and open modes of operations are modelled as follows:

$$\dot{x}_1 = A_1 x + B_1 x \quad \text{(when } S_w \text{ is ON)} \tag{3.1}$$

$$\dot{x}_2 = A_2 x + B_2 x \quad \text{(when } S_w \text{ is OFF)} \tag{3.2}$$

Where A_1 and A_2 are the state matrix, B_1 and B_2 are the input matrix, x is called the state vector. x_1 and x_2 are the states.

The state equations when S_w is ON:

$$L\frac{di_L}{dt} = V_{in} \quad \text{and} \quad C\frac{dv_c}{dt} = -\frac{V_0}{R} \tag{3.3}$$

Where, i_L is the current of the inductor, which equals to i_{in}; v_c is the voltage across the capacitor which equals to output voltage (V_0).

Let, $x_1 = i_L\,(i_{in})$, and $x_2 = v_c\,(V_o)$ are the state-variables.

The state-space equations when switch is ON is being derived as follows:

$$\begin{bmatrix} \dot{x}_1 \\ \dot{x}_2 \end{bmatrix} = \begin{bmatrix} 0 & 0 \\ 0 & \frac{-1}{RC} \end{bmatrix} \begin{bmatrix} x_1 \\ x_2 \end{bmatrix} + \begin{bmatrix} \frac{1}{L} \\ 0 \end{bmatrix} V_{in} \quad \text{where, } A_1 = \begin{bmatrix} 0 & 0 \\ 0 & \frac{-1}{RC} \end{bmatrix} \text{ and } B_1 = \begin{bmatrix} \frac{1}{L} \\ 0 \end{bmatrix} \tag{3.4}$$

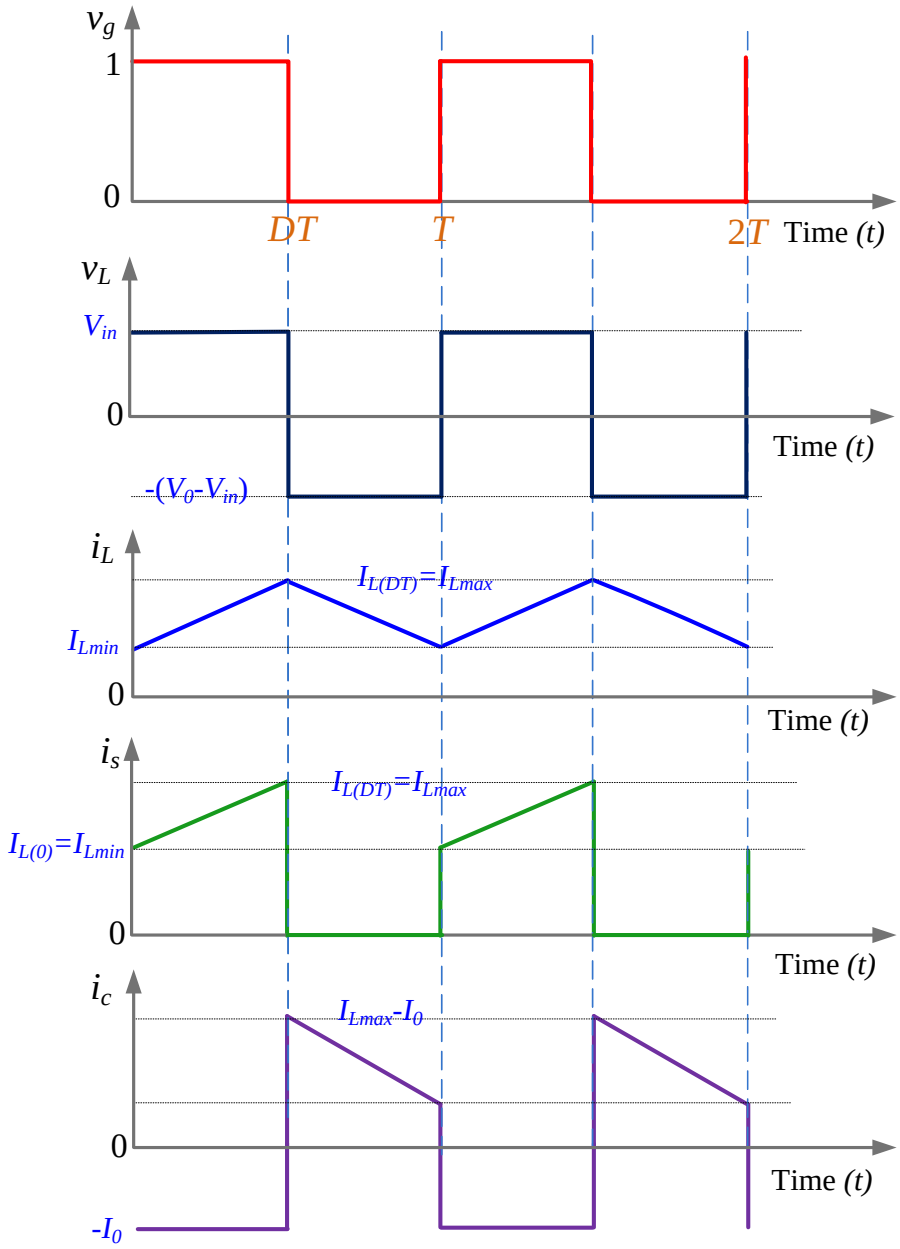

Figure 3-3: *Switching Waveforms of the boost converter in continuous mode.*

The state equations when S_w is OFF are given as follows:

$$L\frac{di_L}{dt} = V_{in} - V_0 \quad \text{and} \quad C\frac{dv_c}{dt} = i_{in} - \frac{V_0}{R} \tag{3.5}$$

The state-space equations when switch is OFF are obtained as follows:

$$\begin{bmatrix} \dot{x}_1 \\ \dot{x}_2 \end{bmatrix} = \begin{bmatrix} 0 & \frac{-1}{L} \\ \frac{1}{C} & \frac{-1}{RC} \end{bmatrix} \begin{bmatrix} x_1 \\ x_2 \end{bmatrix} + \begin{bmatrix} \frac{1}{L} \\ 0 \end{bmatrix} V_{in} \quad \text{where, } A_2 = \begin{bmatrix} 0 & \frac{-1}{L} \\ \frac{1}{C} & \frac{-1}{RC} \end{bmatrix} \text{ and } B_2 = \begin{bmatrix} \frac{1}{L} \\ 0 \end{bmatrix} \tag{3.6}$$

Now, averaging the state-space matrix using (3.1) and (3.2), for switching-ON and OFF working modes. The modified state-space average model is obtained as (3.7) [49]**.**

$$\begin{bmatrix} \dot{x}_1 \\ \dot{x}_2 \end{bmatrix} = \begin{bmatrix} 0 & \frac{-(1-D)}{L} \\ \frac{(1-D)}{C} & \frac{-1}{RC} \end{bmatrix} \begin{bmatrix} x_1 \\ x_2 \end{bmatrix} + \begin{bmatrix} \frac{1}{L} \\ 0 \end{bmatrix} V_{in} \quad \text{where, } \bar{A} = \begin{bmatrix} 0 & \frac{-(1-D)}{L} \\ \frac{(1-D)}{C} & \frac{-1}{RC} \end{bmatrix} \text{ and } \bar{B} = \begin{bmatrix} \frac{1}{L} \\ 0 \end{bmatrix} \tag{3.7}$$

Where, $\bar{A}$ and $\bar{B}$ are the combination of the A_1 and A_2 and B_1 and B_2**,** respectively.

3.2 Selection of the components

3.2.1 Switching Frequency*(f_s)*

Selecting the proper switching frequency was the first step in the design process. A much higher switching frequency reduces acoustic noise and the size of the inductor and the capacitor. However, this increases the switching losses, thereby decreasing the total efficiency of the regulator. The switching frequency (f_s) selected for this purpose is 50kHz.

3.2.2 Inductor Selection*(L)*

The inductor acts as the magnetic field storage element. Selection of the inductor value is done so that it allows the maximum ripple current at minimum value of *D*. The ripple current in the inductor is assumed to be 5%. The designed inductor value is calculated as follows [50]:

$$L_{\min} = \left[\frac{D(1-D)^2 R}{2 f_s} \right] \tag{3.8}$$

$$L = L_{\min} + 5\% L_{\min} \tag{3.9}$$

where, L_{min} is the minimum inductance value and *L* is the inductor, *D* is the duty cycle, *R* is the load resistance, f_s is the switching frequency. *D* is 0.5 and *R* is 53 **Ω**, for selecting the value of *L* and *C*.

3.2.3 Capacitor Selection

The capacitor is required to smoothen the load voltage ripple and serves as an energy source during load transients [50]. The designed capacitor value is evaluated as (3.10). Where, *r* is the ripple factor. In this study, the value of *r* is 5**%.**

$$C = \frac{D}{r R f_s} \tag{3.10}$$

4 Proposed Roach Infestation Optimization (RIO) Based MPPT Algorithm

4.1 An overview of Particle swarm optimization (PSO)

Particle swarm optimization (PSO) is a stochastic optimization method developed by Dr. Eberhart and Dr. Kennedy in 1995, which is motivated by the social behaviour of bird flocking or fish schooling or swarming theories [51]. Each individual in this algorithm, is initialized as a particle, flies in the problem space, and searches for the optimal position.

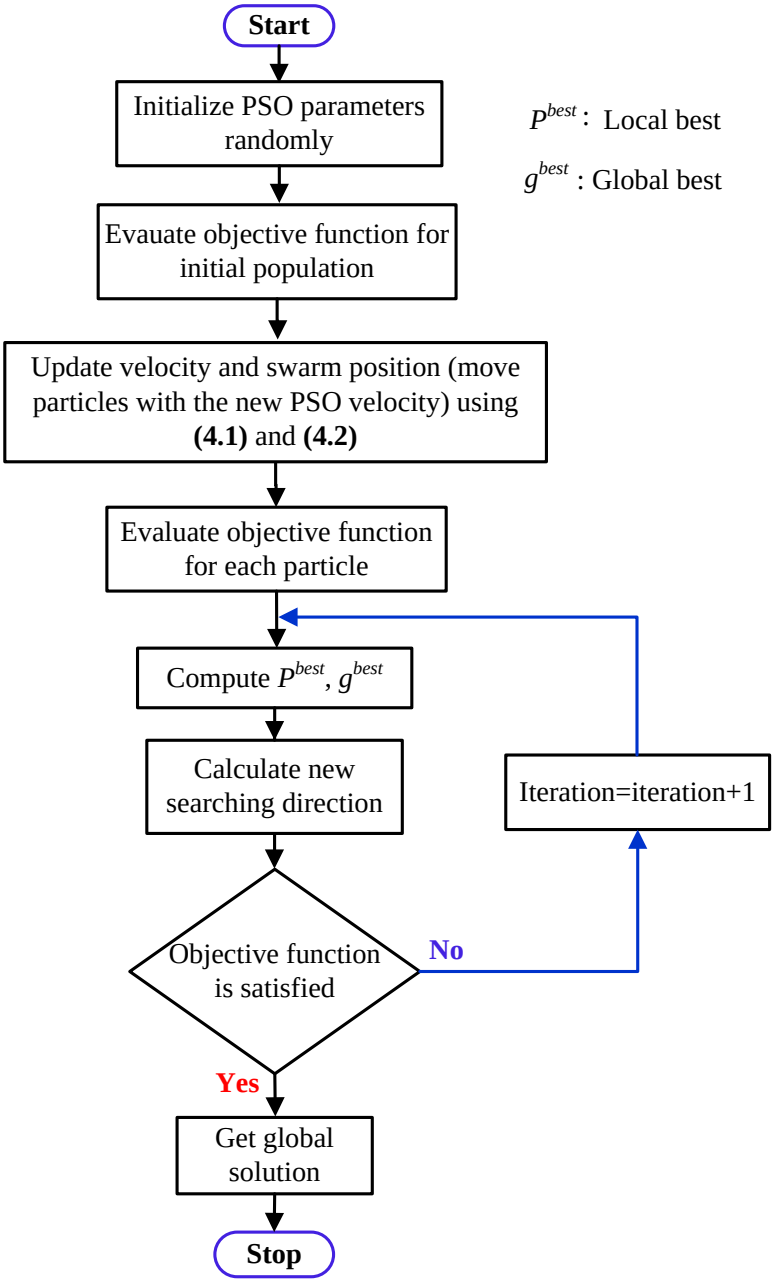

Figure 4-1: *Flowchart of PSO algorithm*

The position of each particle is considered a solution to the problem. To find the best position at each time, the particles move around changing their velocity and position in the search space. They change their position based on their neighboring particle's experience at the past moment of the flight with time. Based on this phenomenon, a mathematical equation for updating the position and velocity of the particles is shown as follows [51]:

$$v_i^{l+1} = w\, v_i^l + c_1 r_1 * \left(P_i^{best} - x_i^l \right) + c_2 r_2 * \left(g_i^{best} - x_i^l \right) \tag{4.1}$$

$$x_i^{l+1} = x_i^l + v_i^{l+1} \tag{4.2}$$

where, * is an operator which is element-by-element vector multiplication. v^l_i represents the velocity of i^{th} particle for the l^{th} iteration. x^l_i represents the position of i^{th} particle for the l^{th} iteration. P^{best} represents the best position of i^{th} particle. g^{best} is the best particle position among the entire particle in the population or swarm. r_1 and r_2 are the random numbers with values lies between [0, 1]. w is weight parameter. c_1 and c_2 are the acceleration constants which are known as the cognitive parameter and social parameter, respectively which values lies between [0, 1]. **Figure 3.1** shows the PSO algorithm's flowchart.

4.2 Proposed Roach Infestation Optimization Algorithm

RIO was originally introduced by Haven et al., as a cockroach inspired algorithm [52]. RIO was adapted from the traditional PSO algorithm, and therefore it has some parameters similar to PSO. A hungry version of PSO and RIO were also described. It is assumed that cockroaches begin as individuals and are governed by only the find dark behavior [52]. Whenever a cockroach encounters another neighboring cockroach, it stops and socializes. During this period, information about the darkest known location is shared. When a cockroach is hungry it leaves friends and comfortable shelter and searches for food. A hunger counter is defined for each cockroach agent, and once it is reached, the cockroach is transported to a food location within the search region. The find food behaviour causes population diversity; this prevents local convergence. RIO is described with three behaviours:

1. *Find the darkest location:* Cockroaches search for the darkest location in the search space, and the fitness value is directly proportional to the level of darkness. The equation that models to find the Darkness behaviour is as follows [52]:

$$v_i^{l+1} = C_0 v_i^{\,l} + C_{\max} R_1 * (p_i^{\,best} - x_i^{\,l}) \tag{4.4}$$

where v^l_i represents the velocity of i^{th} particle for the l^{th} iteration, x^l_i is the current location for the l^{th} iteration, p_i^{best} is the best location found by the i^{th} agent, C_o and C_{max} are constants and R_1 is a vector of uniform random numbers. * is an operator which is element-by-element vector multiplication. This equation emulates Find darkness because $(p_i^{best} - x_i)$ is a velocity change in the direction of the darkest known location for that agent.

2. *Find friend:* If a cockroach comes within a detection radius of another cockroach, it stops, socialize and share information of the darkest known location by setting local location g_i^{best}

$$g_i^{best} = \arg\min\{\text{Function}(p_k)\}, k = \{i, j\} \quad (4.5)$$

Where (i, j) are the indices of the two socializing cockroaches and p_k is the darkest known location for the individual cockroach agent (personal best). Now equation (4.4) can be extended as:

$$v_i^{l+1} = c_0 v_i^l + c_{\max} r_i * (P_i^{best} - x_i^l) + c_{\max} r_2 * (g_i^{best} - x_i^l) \quad (4.6)$$

3. *Find food:* When a cockroach experiences hunger, it leaves the comfort of friends to search for food and is taken to a food source b that is positioned randomly in the search region.

$$x_i = b \quad (4.7)$$

b is the random food location.

Table 4-1: Parameters for PSO and RIO algorithms

Optimization algorithm	parameter	value
PSO		
Cognitive parameter	c_1	1.2
Social parameter	c_2	1.6
Weight parameter	w	0.4
RIO		
Cockroach parameter	C_0	0.4
Cockroach parameter	C_{max}	1.4

To attain the results, the parameters of the PSO and RIO optimization algorithms are stated in **Table 4.1**. Furthermore, the boost DC-DC converter receives the PV voltage (V_{pv}) and current (I_{pv}) from the PV system and subsequently regulates it by adjusting the duty cycle (D) to achieve the maximum power point (MPP tracker) as shown in **Figure 5.1** which is given in the next Section. The global peak power (G_P) of the PV system is obtained using the optimization algorithm to update D in the search process during uniform irradiation/temperature and PSCs. The flowchart of the proposed RIO algorithm for MPPT is presented in **Figure 4.2**.

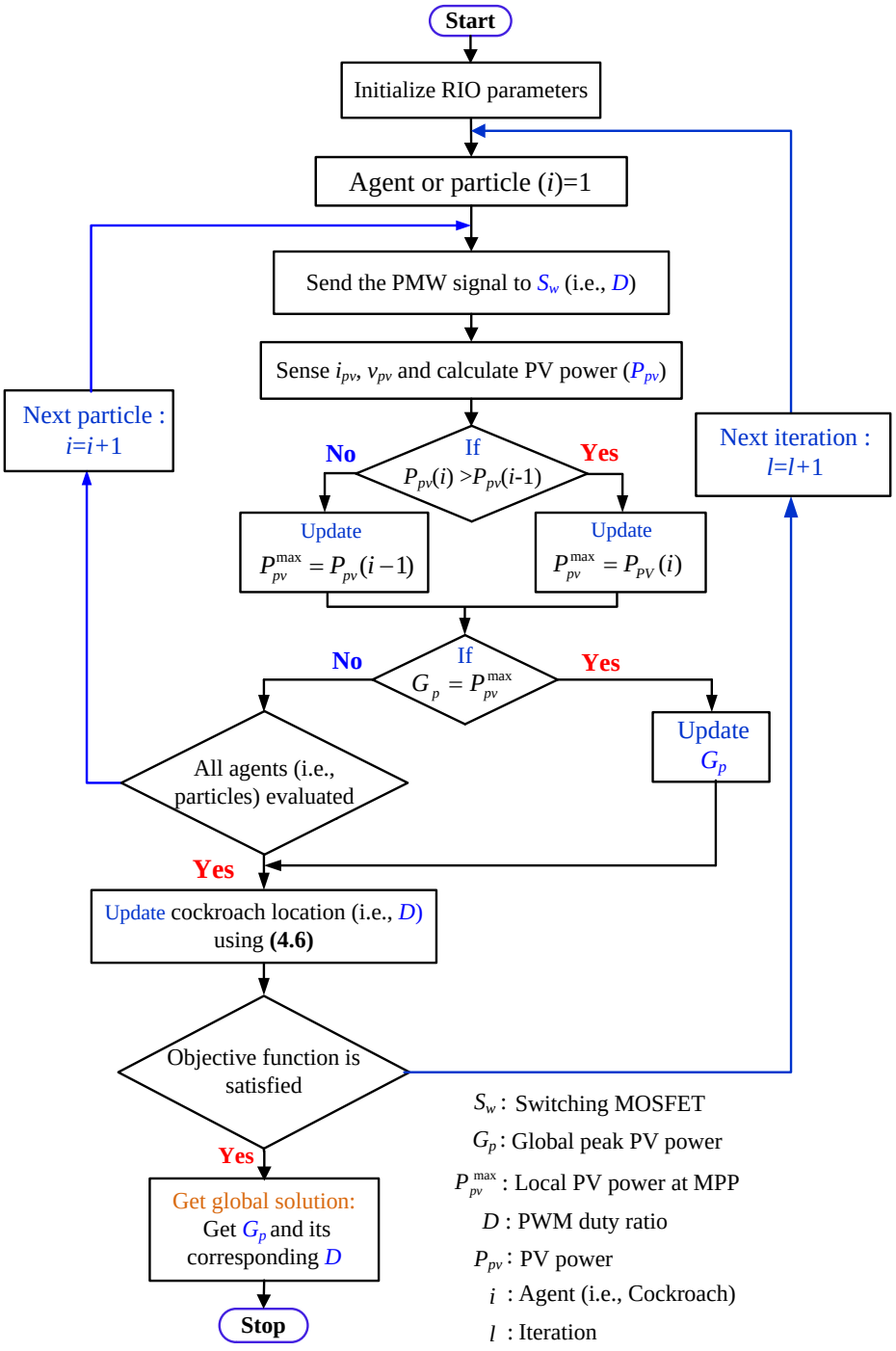

Figure 4-2: *Flowchart of proposed RIO algorithm for MPPT*

5 Results and Discussions

A MATLAB/Simulink (R2020b) software is used for modeling and to validate the performance of the proposed MPPT technique of the PV system. The PV system (PVS) consists of four-series (4S) connected PV modules, a resistive load, and a non-isolated DC-DC boost converter with the MPPT technique. The MATLAB/Simulink model of the studied PVS is shown in **Figure 5.1**. The simulation modelling parameters used for the PVS and DC-DC converter are given in **Table-5.1**.

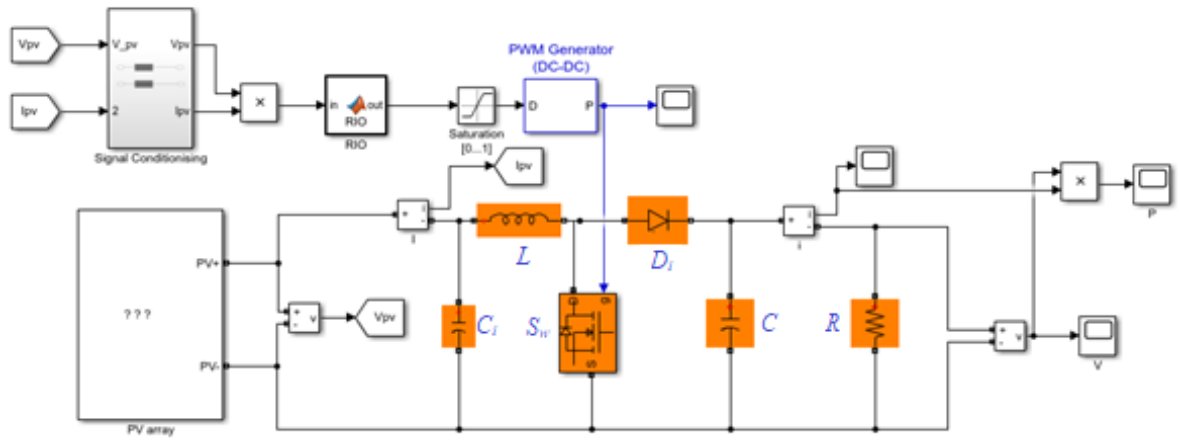

***Figure 5-1**: Simulink diagram of PV system*

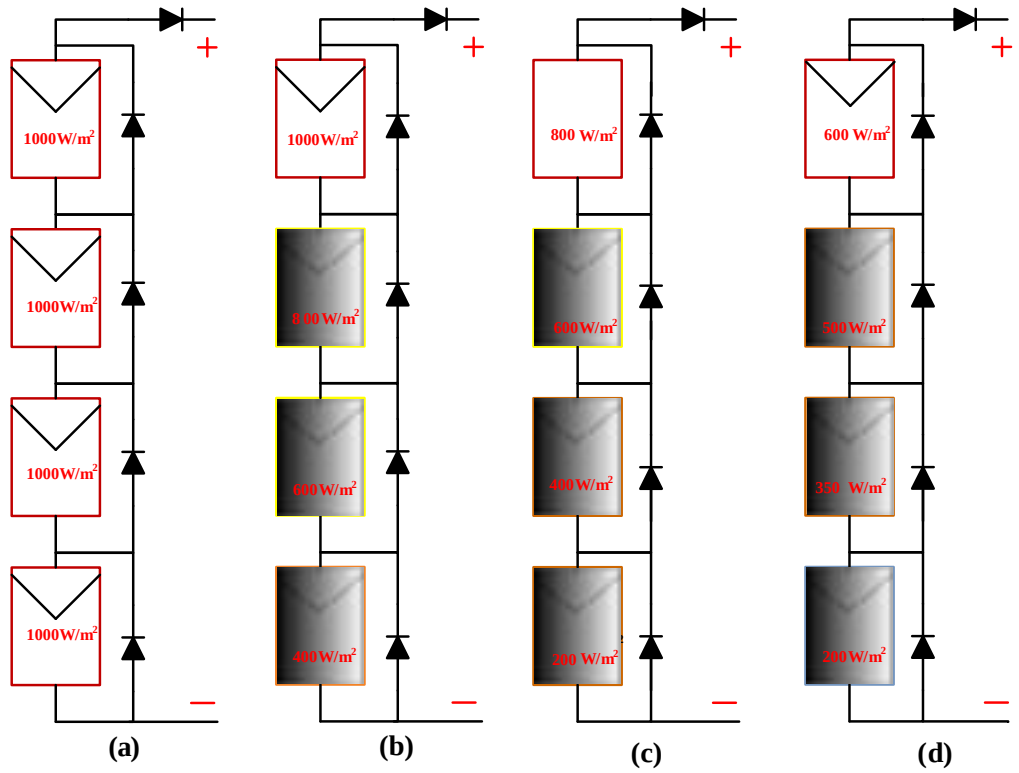

***Figure 5-2:** 4S structure of PV system **(a).** Pattern-1, **(b).** Pattern-2, **(c).** Pattern-3, **(d).** Pattern-4*

Table 5-1: *PV system and DC-DC converter Parameters*

System parameters/data	Symbol	Value
For one PV module		
Maximum power for1000W/m^2 and 25^{0}C	P_{pv}^{max}	59.85W
Voltage at MPP for 1000W/m^2 and 25^{0}C	V_{pv}^{max}	17.1V
Current at MPP for1000W/m^2 and 25^{0}C	I_{pv}^{max}	3.5A
Open-circuit voltage	V_{oc}	21.1V
Short-circuit current	I_{sc}	3.8A
Series resistance	R_s	0.10363 Ω
Shunt resistance	R_{sh}	283.3724 Ω
Ideality factor	A_0	1.5406
Temperature co-efficient of *Isc*		0.00247 %/°C
Temperature co-efficient of V_{oc}		-0.8 %/°C
Boost converter parameters (Figure-5.1)		
Capacitor	C	464µF
Input filter capacitor	C_i	10µF
Inductor	L	1.14mH
Switching frequency	f_s	50kHz
Load resistance	R	53 Ω

Table 5-2: *Various shading Pattern of PVS for different solar irradiation (G)*

Shading pattern	Module-1: *G* in (W/m^2)	Module-2: *G* in (W/m^2)	Module-3: *G* in (W/m^2)	Module-4: *G* in (W/m^2)
Pattern-1	10000	1000	1000	1000
Pattern-2	1000	800	600	400
Pattern-3	800	600	400	200
Pattern-4	600	500	350	200

To validate the effectiveness of the proposed RIO algorithm based MPPT the time-domain simulations have been carried out for both uniform irradiation and PCS operating conditions such as **(i).** uniform irradiance (Pattern-1) and **(ii).** PSCs (Pattern-2 to Pattern-4) as shown in **Figure 5.2**. For the case of uniform irradiance, the values of irradiance and temperature are kept constant, whereas, in the case of PSCs, the irradiance values of the PV modules are considered. **Table 5.2** shows the combination on various patterns selected for the PVS to plot the graphs. The PVS is simulated under the various scenarios which are discussed below:

Case 1: P-V and I-V characteristics curves of the PV system at 25^0C

The performance of a solar panel affects under both uniform irradiation/temperature and PSCs. The PV system, whether a module, string or array exhibits a *P-V* curve exhibiting multiple peaks, a Global Maximum Power Point (GMPP) which is the highest peak and Local Maximum Power Points (LMPPs) are the other multiple peaks. The *P-V* and *I-V* graphs under each pattern is given below from figure 5.3 to figure 5.6. it is seen that, when under uniform conditions (i.e., pattern-1), the *P-V* and *I-V* graphs produce only one maximum point. However, when partial shading (i.e., pattern-2 to pattern-4) occurs in the PVS, the *P-V* and *I-V* graphs starts producing multiple maximum points due to the working of the bypass Diodes in the system. The corresponding results for the peak power is shown in **Table 5.3**.

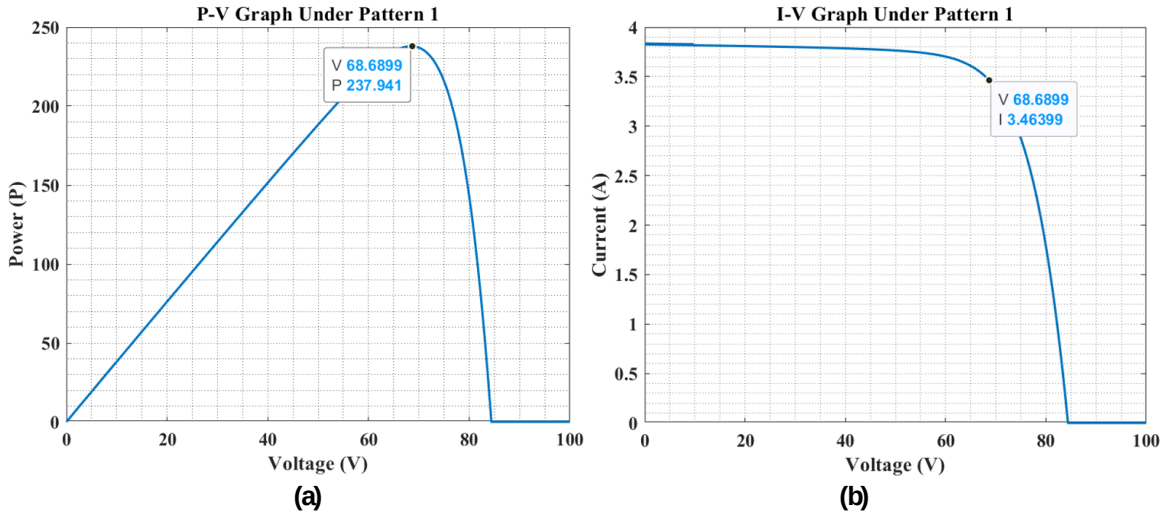

Figure 5-3: *Graph for pattern-1 at 25^0C* ***(a).*** *P-V curve and* ***(b).*** *I-V curve*

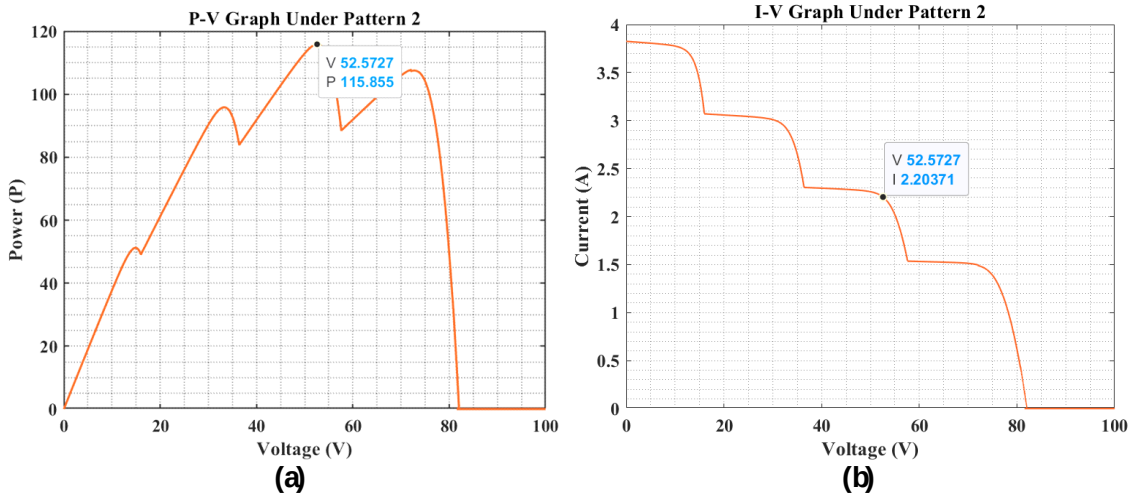

Figure 5-4: *Graph for pattern-2 at 25^{0}C* ***(a).*** *P-V curve and* ***(b).*** *I-V curve*

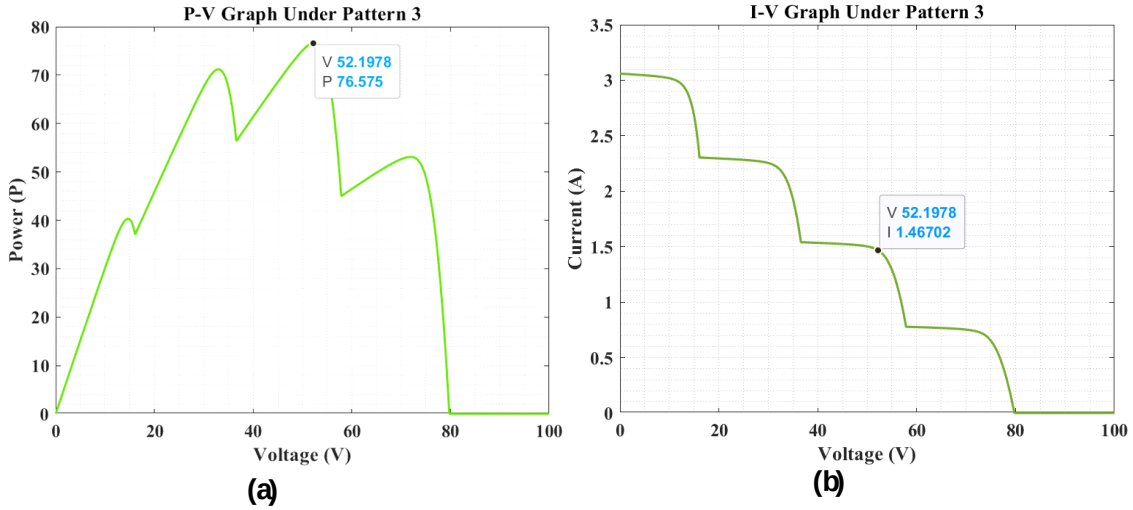

Figure 5-5*: Graph for pattern-3 at 25^{0}C* ***(a).*** *P-V characteristics and* ***(b).*** *I-V characteristics*

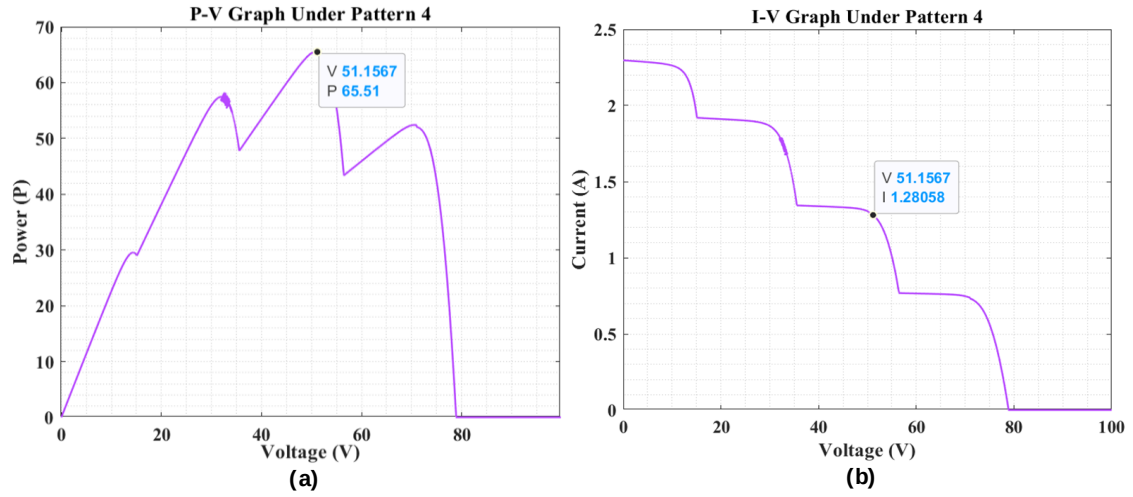

Figure 5-6: *Graph for pattern-4 at 25^{0}C* ***(a).*** *P-V curve and* ***(b).*** *I-V curve*

***Case 2**: P-V and I-V characteristics curves of the PV system at 20^0C*

To show the effect of temperature on the *P-V* and *I-V* characteristics plots, the same PSCs are considered which is presented in *Case-1* at 20^0C. The *P-V* and *I-V* characteristics plots at 20^0C are shown in **Figures 5.7** to **5.10** for each PSC pattern, respectively. From the graphs (**Figures 5.3** to **5.10**), it is seen that in *Case-2* the power of the PVS increases as compared to *Case-1*. This validates the fact that the decrease in temperature on a PV cell increases the performance (i.e., high power or/and efficiency) of the PV cell and vice versa. The exact value of the global peak power (G_p) of the PVS under the selected test patterns for both temperatures are given in **Table-5.3**.

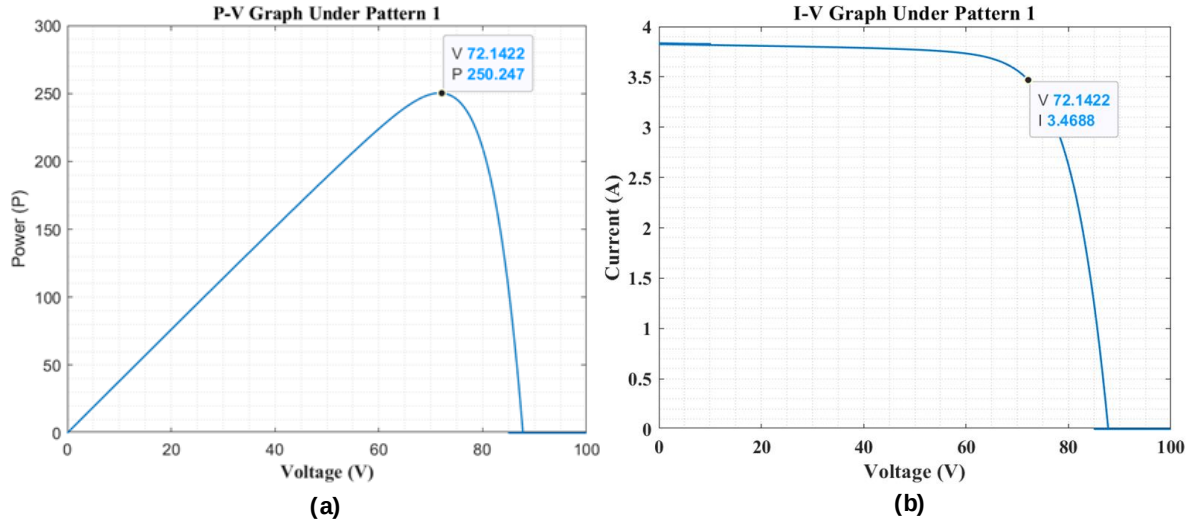

***Figure 5-7**: Graph for pattern-1 at 20^0C **(a).** P-V curve and **(b).** I-V curve*

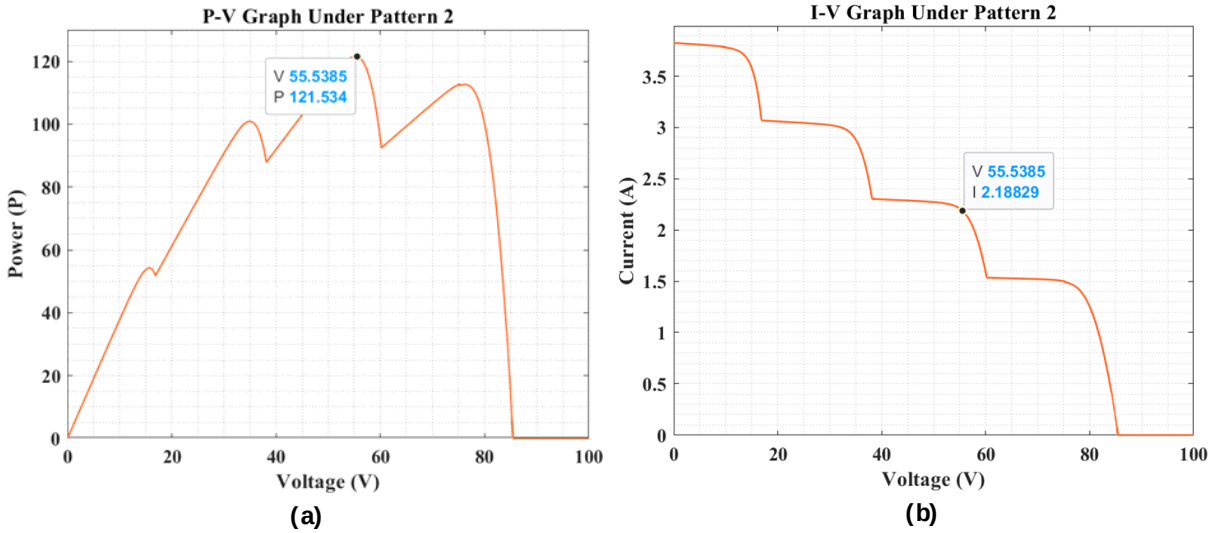

***Figure 5-8:** Graph for pattern-2 at 20^0C **(a).** P-V curve and **(b).** I-V curve*

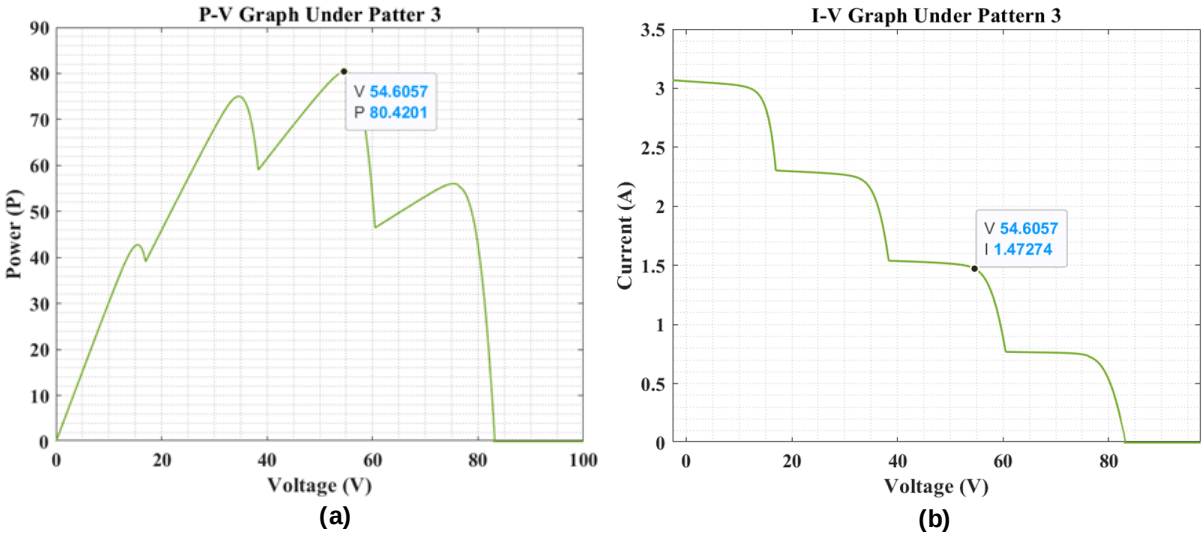

Figure 5-9: *Graph for pattern-3 at 20^{0}C* ***(a).*** *P-V curve and* ***(b).*** *I-V curve*

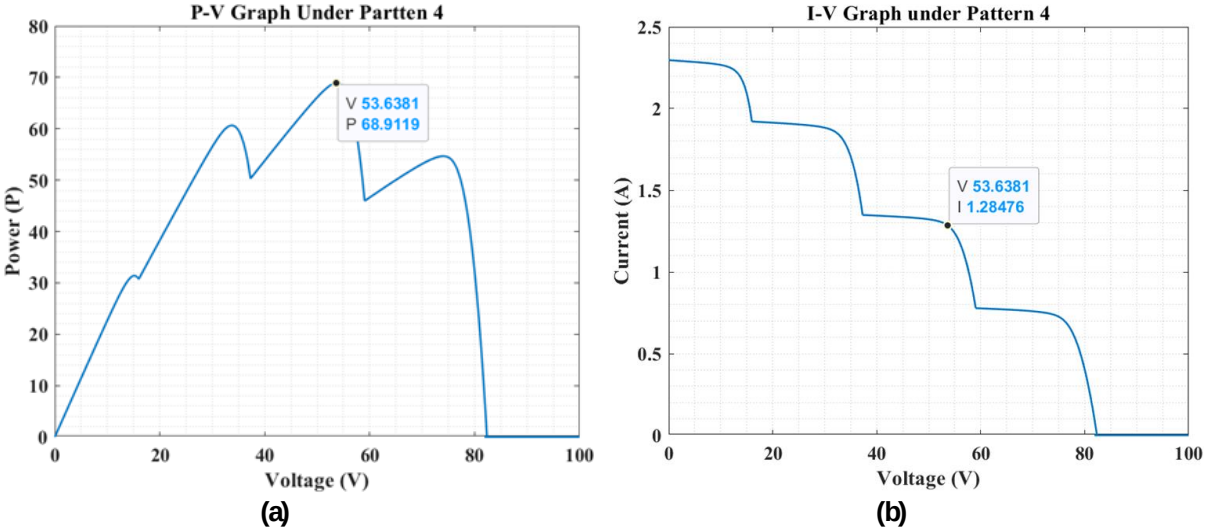

Figure 5-10: *Graph for pattern-4 at 20^{0}C* ***(a).*** *P-V curve and* ***(b).*** *I-V curve*

Table 5-3: *Comparative global peak power (G_p) of the PVS under the selected test Patterns*

Pattern	PV maximum power (P_{max}) @ 25^{0}C	PV maximum power (P_{max}) @ 20^{0}C
Pattern-1	237.941W	250.247W
Pattern-2	115.855W	121.534W
Pattern-3	76.575W	80.420W
Pattern-4	63.668W	68.912W

The global peak power (G_p) of the PVS for is given in the **Table 5.3**.

Case 3: *Comparison between PSO and proposed RIO algorithm*

To ensure satisfactory performance under partial shading, the proposed MPPT identifies the GMPP. For GMPP tracking, the V_{pv} and the I_{pv} are significant for identifying the MPP. The actual PV power (P_{pv}), PV voltage (V_{pv}), PV current (I_{pv}), and output voltage of the boost converter(V_0) are presented based on the results obtained from both PSO and proposed RIO algorithms. This simulation results are carried out under the same patterns and temperature of 25^0C as taken in *Case-1*.

As shown in **Figures 5.11** and **5.12** the RIO MPPT technique tracked the MPP of the system better than the PSO. This performance of the RIO technique was confirmed by comparing the results with that of the PSO.

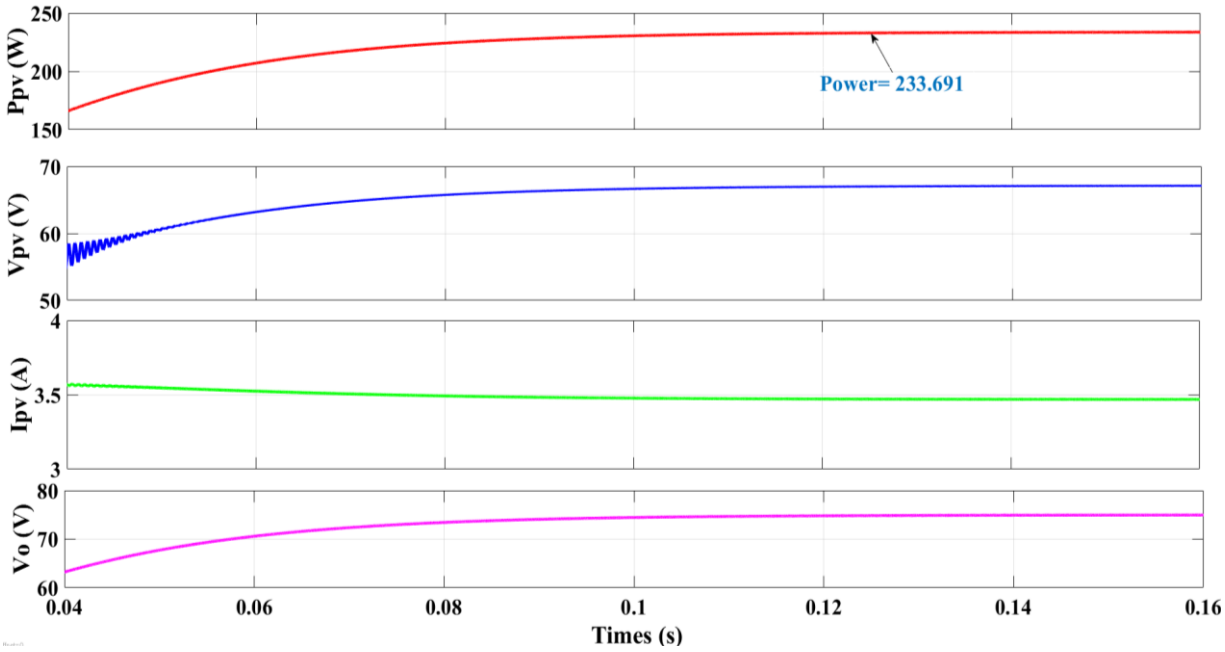

Figure 5-11: *Performance graphs of PV system under Pattern-1 for PSO algorithm*

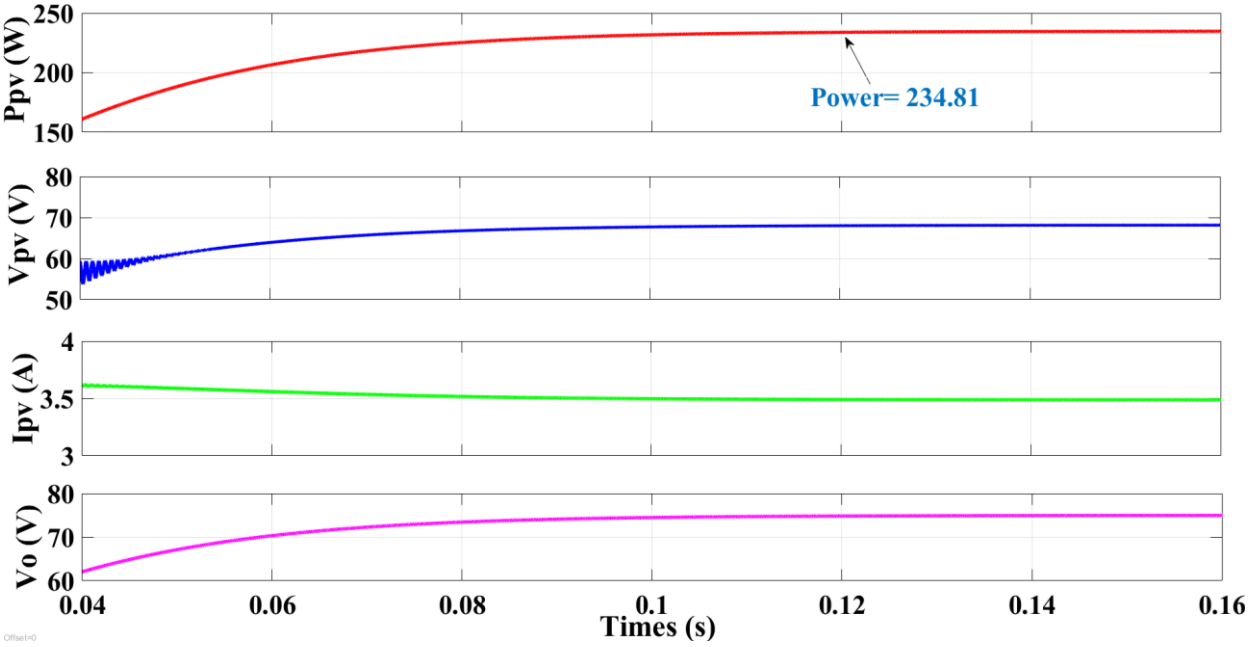

Figure 5-12: *Performance graphs of PV system under Pattern-1 for RIO algorithm*

Under pattern-2, the RIO was able to track a higher MPP than the PSO. The Ppv tracked by the RIO was 113.886*W* as compared to 113.60 *W* by the PSO. The corresponding results are shown in the figure 5.13 and 5.14..

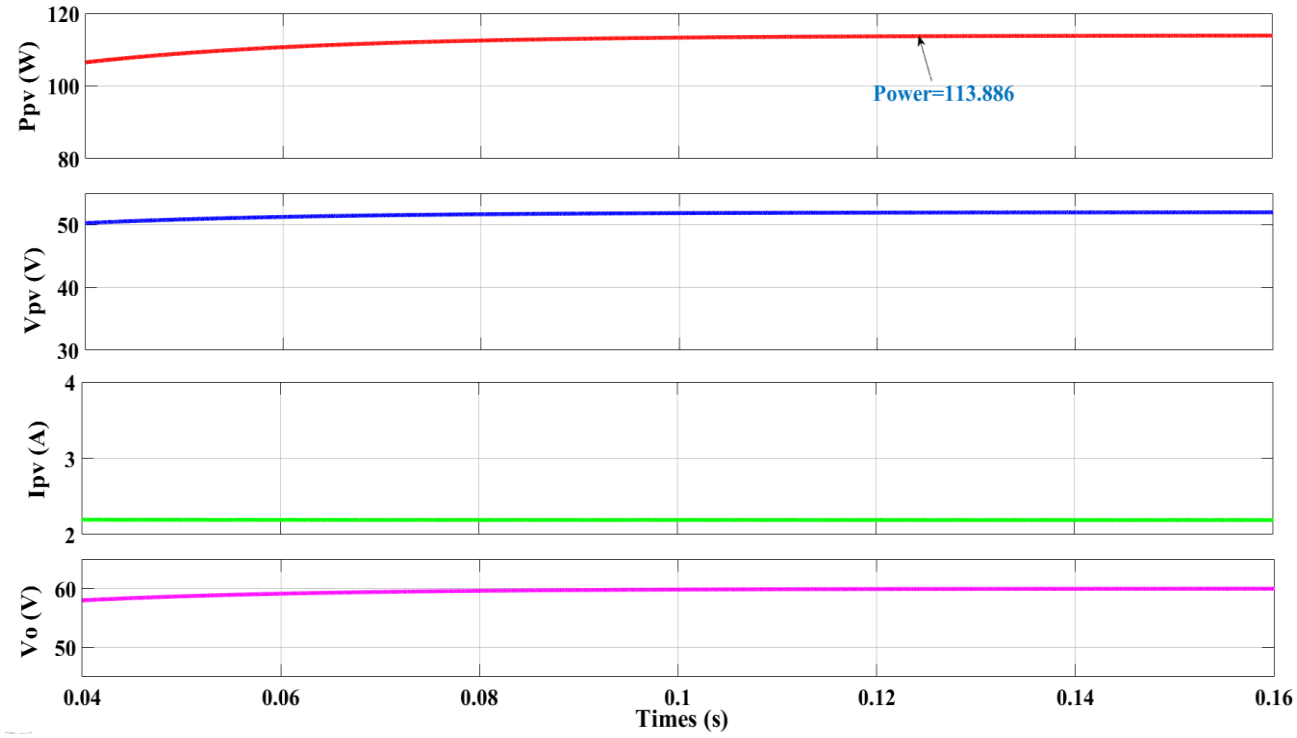

Figure 5-13: *Performance graphs of PV system under Pattern-2 for RIO algorithm*

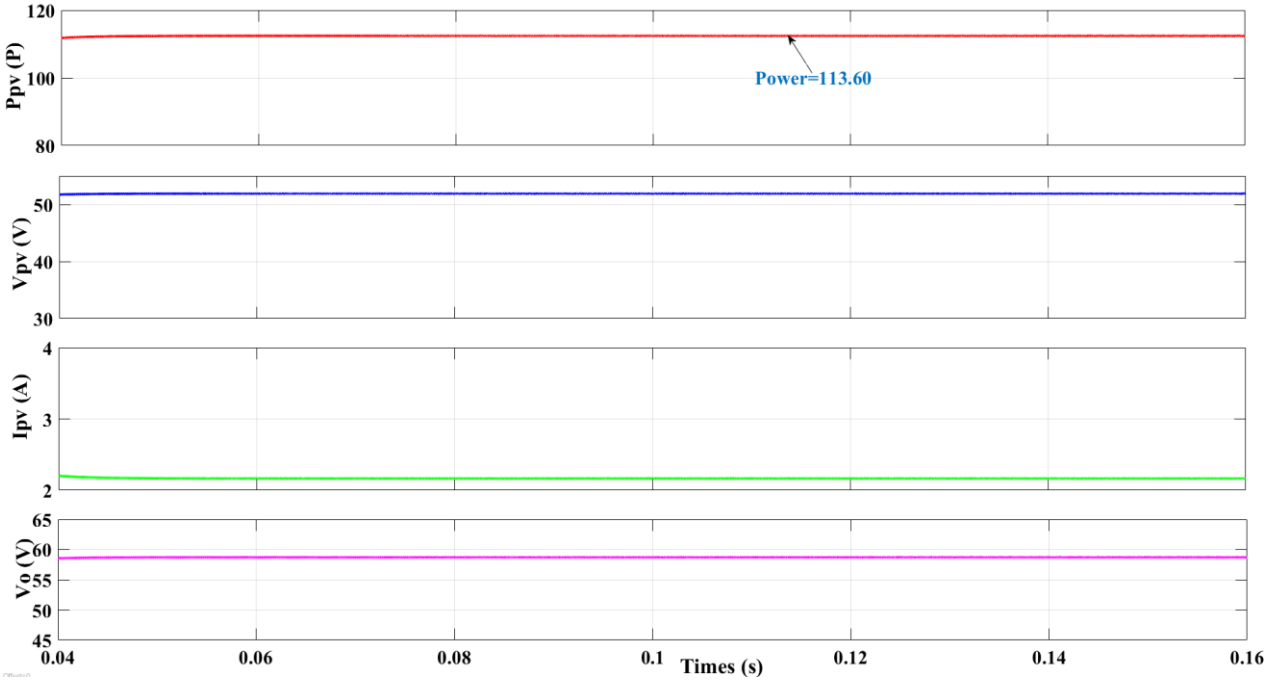

Figure 5-14: *Performance graphs of PV system under Pattern-2 for PSO algorithm*

Under Pattern-3, the RIO outperformed the PSO again by tacking $75.1625W$ as compared to $74.978W$ of the MPP. The corresponding results are shown in the figure below.

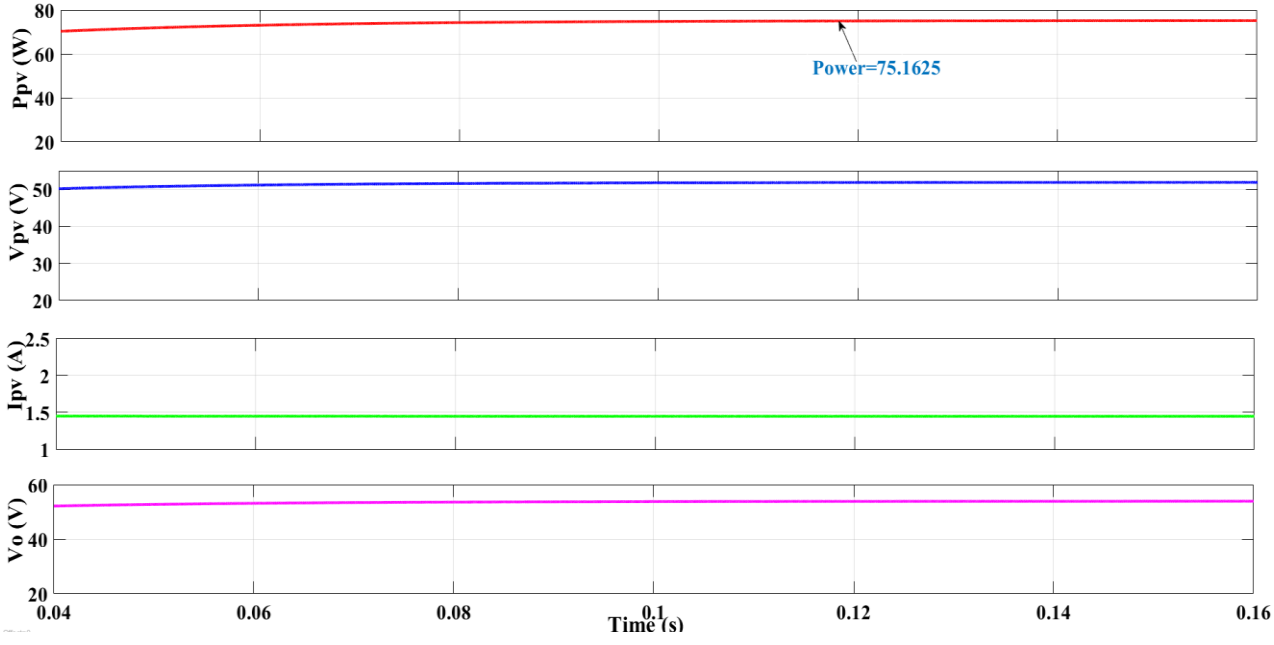

Figure 5.15*: Performance graphs of PV system under Pattern-3 for RIO algorithm*

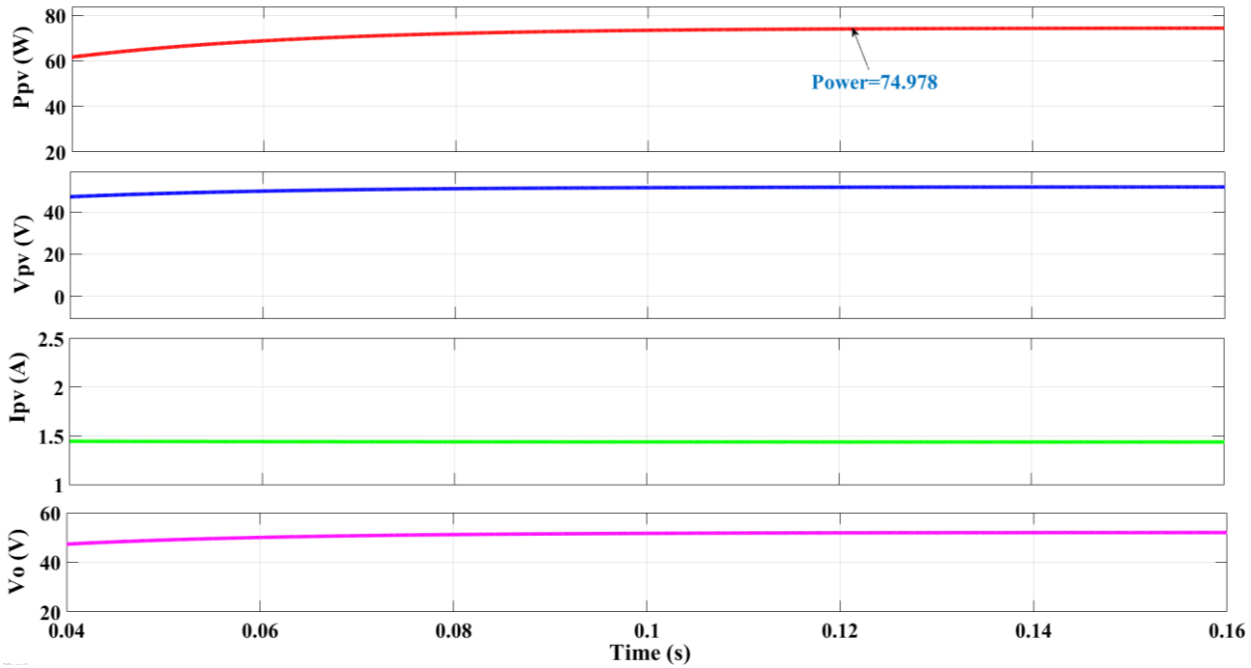

Figure 5-15: *Performance graphs of PV system under Pattern-3 for PSO algorithm*

In pattern-4, the RIO was able to track a higher MPP than the PSO. The Ppv tracked by the RIO was 64.267W as compared to 64.1382W by the PSO. The corresponding results are shown in the figure below.

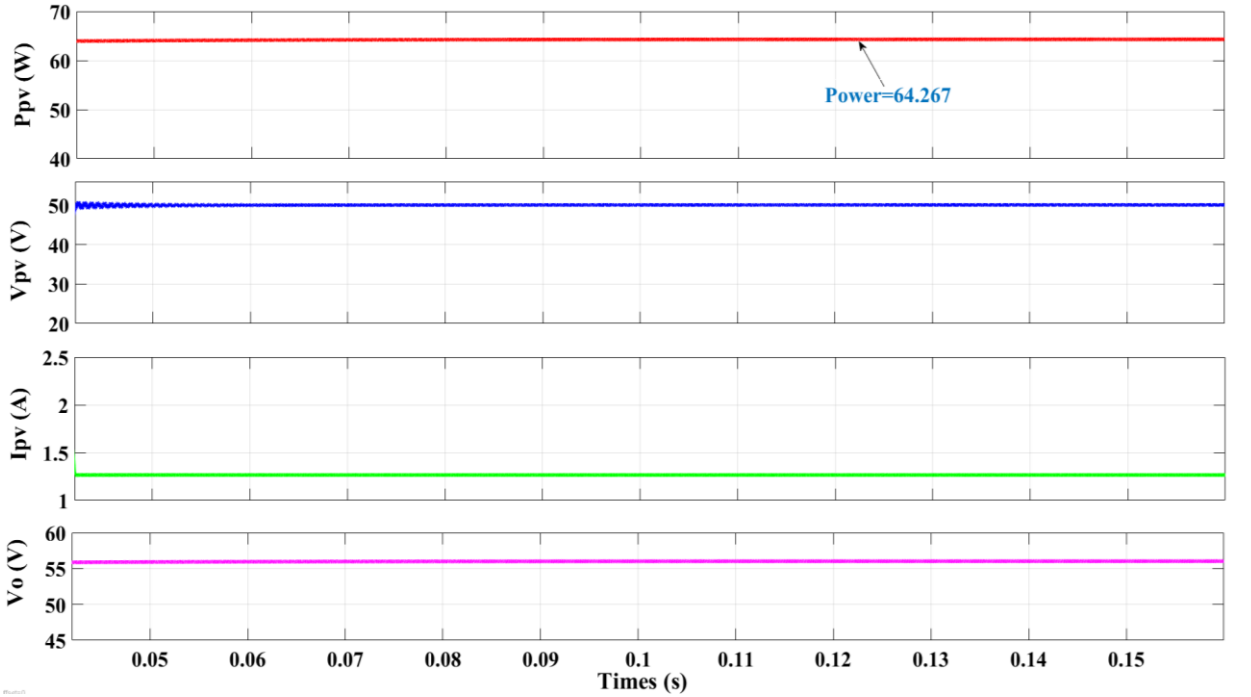

Figure 5.17*: Performance graphs of PV system under Pattern-4 for RIO algorithm*

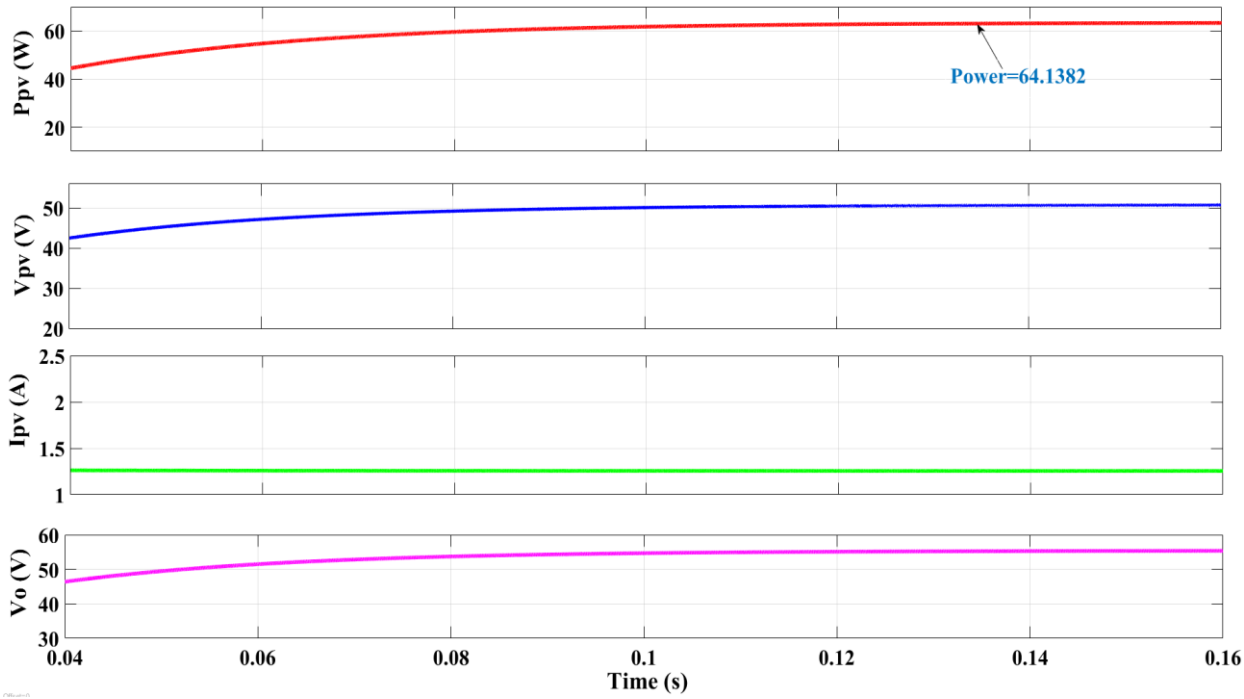

Figure 5.18: *Performance graphs of PV system under Pattern-4 for PSO algorithm*

To achieve the actual performance attained by both algorithms, the effectiveness of the MPPT-algorithms is benchmarked using the MPPT efficiency (ηMPPT) equation as follows:

$$\%\,\eta_{MPPT} = \frac{P_{pv}}{P_{MPPT}} \times 100 \tag{5.1}$$

where, P_{MPPT} is the maximum achievable power or true MPP of the PV system (maximum power points is shown in **Figures 5.3** to 5**.10**). $P_{pv,}$ is the actual power extracted from the PV array which depends upon the ability of the MPPT to be as close as possible to true MPP system (**Figures 5.11** to 5**.18**). The higher the MPPT algorithm's accuracy, the higher the η_{MPPT}. The tracking efficiency of the MPPT algorithms for the PV system is shown in **Table 5.4.** From the above results, it can be concluded that the proposed RIO technique has a good tracking competency as compared to the PSO-based MPPT technique. Moreover, it can be observed that η_{MPPT} varies with change in PCS pattern as the search behaviour of the optimization algorithms are random in nature to track the optimal point. The results showed the robustness of the RIO algorithm.

Table 5-4: *Comparative actual power (P_{pv}) extracted by RIO and PSO*

Patterns	RIO	PSO
Pattern 1	234.81W	233.692 W
Pattern 2	113.886W	113.60 W
Pattern 3	75.1625 W	74.978 W
Pattern 4	64.267 W	64.1382 W

Table 5-5: *Efficiency of RIO and PSO under the various test conditions (ηMPPT)*

Patterns	RIO	PSO
Pattern 1	98.689*%*	98.214*%*
Pattern 2	98.3*%*	98.054*%*
Pattern 3	98.155*%*	97.915*%*
Pattern 4	98.103*%*	97.68*%*

6 Conclusions

In this thesis, an MPPT technique based on a bio-inspired Roach infestation algorithm is proposed to extract the maximum power from a solar PV under partial shading condition using step change in irradiation and variation in temperature. The obtained results were examined and compared with the PSO algorithm. The obtained results demonstrate that the RIO MPPT performs remarkably in tracking with high accuracy as PSO based MPPT.

6.1 Scope for Future Work

1. Deployment of the Arduino or FPGA board (i.e., Hardware implementation) to validate the MPPT algorithm in the future.
2. In future, a real PV system can be considered to validate the detailed dynamic performances of the system.
3. Based on this, different converter and inverter topologies could be further developed.

6.2 References

[1] https://www.bp.com/content/dam/bp/pdf/energy-economics/energy-outlook2017/bp-energy-outlook-2017.pdf (accessed 20th April, 2021).

[2] M. Jaganmohan. "Global cumulative installed solar PV capacity 2000-2019." https://www.statista.com/statistics/280220/global-cumulative-installed-solar-pv-capacity/ (accessed February, 24, 2021).

[3] "Renewable energy production in Norway." Government.no. https://www.regjeringen.no/en/topics/energy/renewable-energy/renewable-energy-production-in-norway/id2343462/ (accessed 22nd April, 2021).

[4] H. R. a. M. Roser. "Norway: Energy Country Profile." ourworldInData.org. https://ourworldindata.org/energy (accessed 22nd APril, 2021).

[5] "ELECTRICITY PRODUCTION." Norwegian Ministry of Petroleum and Energy. https://energifaktanorge.no/en/norsk-energiforsyning/kraftproduksjon/ (accessed 23 April, 2021).

[6] N. Amin, S. Ahmad Shahahmadi, P. Chelvanathan, K. S. Rahman, M. Istiaque Hossain, and M. D. Akhtaruzzaman, "Solar Photovoltaic Technologies: From Inception Toward the Most Reliable Energy Resource," in *Encyclopedia of Sustainable Technologies*, M. A. Abraham Ed. Oxford: Elsevier, 2017, pp. 11-26.

[7] "Solar PV Electricity Generation." Solar Shams. http://solarshams.com/content/solar-pv-electricity-generation (accessed february, 23th, 2021).

[8] Z. Salam, J. Ahmed, and B. S. Merugu, "The application of soft computing methods for MPPT of PV system: A technological and status review," *Applied Energy*, vol. 107, pp. 135-148, 2013/07/01/ 2013, doi: https://doi.org/10.1016/j.apenergy.2013.02.008.

[9] "Solar Photovoltaic Panel." https://www.alternative-energy-tutorials.com/photovoltaics/photovoltaic-panel.html (accessed 15 May, 2021).

[10] S. Malathy and R. Ramaprabha, "Comprehensive analysis on the role of array size and configuration on energy yield of photovoltaic systems under shaded conditions," *Renewable and Sustainable Energy Reviews*, vol. 49, pp. 672-679, 2015/09/01/ 2015, doi: https://doi.org/10.1016/j.rser.2015.04.165.

[11] M. Amin, J. Bailey, C. Tapia, and V. Thodimeladine, "Comparison of PV array configuration efficiency under partial shading condition," in *2016 IEEE 43rd Photovoltaic Specialists Conference (PVSC)*, 5-10 June 2016 2016, pp. 3704-3707, doi: 10.1109/PVSC.2016.7750368.

[12] T. Andrianajaina, E. Sambatra, C. Andrianirina, T. D. Razafimahefa, and N. Heraud, *Modeling, analysis and comparison of shading effects in a photovoltaic array using different configurations*. 2017.

[13] Salingberbag. "Solar Cells." http://sunpowercell.blogspot.com/2010/09/equivalent-circuit-of-solar-cell.html (accessed March, 29, 2021).

[14] "Kirchhoff's Current Law." https://www.electronics-tutorials.ws/dccircuits/kirchhoffs-current-law.html (accessed 26th April, 2021).

[15] S. Satpathy, "PHOTOVOLTAIC POWER CONTROL USING MPPT AND BOOST CONVERTER," May, 2012 2012.

[16] M. Seyedmahmoudian *et al.*, "State of the art artificial intelligence-based MPPT techniques for mitigating partial shading effects on PV systems – A review," *Renewable and Sustainable Energy Reviews*, vol. 64, pp. 435-455, 2016/10/01/ 2016, doi: https://doi.org/10.1016/j.rser.2016.06.053.

[17] D. Rossi, M. Omana, D. Giaffreda, and C. Metra, "Modeling and Detection of Hotspot in Shaded Photovoltaic Cells," *IEEE Transactions on Very Large Scale Integration (VLSI) Systems*, vol. 23, pp. 1-1, 07/18 2014, doi: 10.1109/TVLSI.2014.2333064.

[18] A. F. de Paulo and G. S. Porto, "Evolution of collaborative networks of solar energy applied technologies," *Journal of Cleaner Production*, vol. 204, pp. 310-320, 2018/12/10/ 2018, doi: https://doi.org/10.1016/j.jclepro.2018.08.344.

[19] P. Choudhary and R. K. Srivastava, "Sustainability perspectives- a review for solar photovoltaic trends and growth opportunities," *Journal of Cleaner Production*, vol. 227, pp. 589-612, 2019/08/01/ 2019, doi: https://doi.org/10.1016/j.jclepro.2019.04.107.

[20] M. Kermadi and E. M. Berkouk, "Artificial intelligence-based maximum power point tracking controllers for Photovoltaic systems: Comparative study," *Renewable and Sustainable Energy Reviews*, vol. 69, pp. 369-386, 2017/03/01/ 2017, doi: https://doi.org/10.1016/j.rser.2016.11.125.

[21] P. Bhatnagar and R. K. Nema, "Maximum power point tracking control techniques: State-of-the-art in photovoltaic applications," *Renewable and Sustainable Energy Reviews*, vol. 23, pp. 224-241, 2013/07/01/ 2013, doi: https://doi.org/10.1016/j.rser.2013.02.011.

[22] N. Karami, N. Moubayed, and R. Outbib, "General review and classification of different MPPT Techniques," *Renewable and Sustainable Energy Reviews*, vol. 68, pp. 1-18, 2017/02/01/ 2017, doi: https://doi.org/10.1016/j.rser.2016.09.132.

[23] K. Ishaque and Z. Salam, "A review of maximum power point tracking techniques of PV system for uniform insolation and partial shading condition," *Renewable and Sustainable Energy Reviews*, vol. 19, pp. 475-488, 2013/03/01/ 2013, doi: https://doi.org/10.1016/j.rser.2012.11.032.

[24] Z. Salam and J. Ahmed, "The application of soft computing techniques to improve the performance of maximum power point tracker for PV system during partial shading," in *2014 IEEE 8th International Power Engineering and Optimization Conference (PEOCO2014)*, 24-25 March 2014 2014, pp. 237-242, doi: 10.1109/PEOCO.2014.6814432.

[25] H. J. El-Khozondar, R. J. El-Khozondar, K. Matter, and T. Suntio, "A review study of photovoltaic array maximum power tracking algorithms," *Renewables: Wind, Water, and Solar,* vol. 3, no. 1, p. 3, 2016/02/18 2016, doi: 10.1186/s40807-016-0022-8.

[26] S. Lyden, M. E. Haque, A. Gargoom, and M. Negnevitsky, "Review of Maximum Power Point Tracking approaches suitable for PV systems under Partial Shading Conditions," in *2013 Australasian Universities Power Engineering Conference (AUPEC)*, 29 Sept.-3 Oct. 2013 2013, pp. 1-6, doi: 10.1109/AUPEC.2013.6725344.

[27] B. Subudhi and R. Pradhan, "A Comparative Study on Maximum Power Point Tracking Techniques for Photovoltaic Power Systems," *IEEE Transactions on Sustainable Energy,* vol. 4, no. 1, pp. 89-98, 2013, doi: 10.1109/TSTE.2012.2202294.

[28] M. Mao, L. Cui, Q. Zhang, K. Guo, L. Zhou, and H. Huang, "Classification and summarization of solar photovoltaic MPPT techniques: A review based on traditional and intelligent control strategies," *Energy Reports,* vol. 6, pp. 1312-1327, 2020/11/01/ 2020, doi: https://doi.org/10.1016/j.egyr.2020.05.013.

[29] K. S. Tey and S. Mekhilef, "Modified Incremental Conductance Algorithm for Photovoltaic System Under Partial Shading Conditions and Load Variation," *IEEE Transactions on Industrial Electronics,* vol. 61, no. 10, pp. 5384-5392, 2014, doi: 10.1109/TIE.2014.2304921.

[30] A. Safari and S. Mekhilef, "Simulation and Hardware Implementation of Incremental Conductance MPPT With Direct Control Method Using Cuk Converter," *IEEE Transactions on Industrial Electronics,* vol. 58, no. 4, pp. 1154-1161, 2011, doi: 10.1109/TIE.2010.2048834.

[31] J. Ahmed and Z. Salam, "An improved perturb and observe (P&O) maximum power point tracking (MPPT) algorithm for higher efficiency," *Applied Energy,* vol. 150, pp. 97-108, 2015/07/15/ 2015, doi: https://doi.org/10.1016/j.apenergy.2015.04.006.

[32] R. Rawat and S. Chandel, "Hill climbing techniques for tracking maximum power point in solar photovoltaic systems - A review," *Special Issue of International Journal of Sustainable Development and Green Economics,* vol. 2, pp. 90-95, 01/01 2013.

[33] F. D. Murdianto, M. Z. Efendi, R. E. Setiawan, and A. S. L. Hermawan, "Comparison method of MPSO, FPA, and GWO algorithm in MPPT SEPIC converter under dynamic partial shading condition," in *2017 International Conference on Advanced Mechatronics, Intelligent Manufacture, and Industrial Automation (ICAMIMIA)*, 12-14 Oct. 2017 2017, pp. 315-320, doi: 10.1109/ICAMIMIA.2017.8387609.

[34] G. Li, Y. Jin, M. W. Akram, X. Chen, and J. Ji, "Application of bio-inspired algorithms in maximum power point tracking for PV systems under partial shading conditions – A review," *Renewable and Sustainable Energy Reviews,* vol. 81, pp. 840-873, 2018/01/01/ 2018, doi: https://doi.org/10.1016/j.rser.2017.08.034.

[35] C. Robles, J. Taborda, and O. Rodriguez, "Fuzzy logic based MPPT controller for a PV system," *Energies,* vol. 10, 12/02 2017, doi: 10.3390/en10122036.

[36] S. Mohanty, B. Subudhi, and P. Ray, "A New MPPT Design Using Grey Wolf Optimization Technique for Photovoltaic System Under Partial Shading Conditions," *IEEE Transactions on Sustainable Energy*, vol. 7, pp. 1-8, 10/26 2015, doi: 10.1109/TSTE.2015.2482120.

[37] A. A. Zaki Diab and H. Rezk, "Global MPPT based on flower pollination and differential evolution algorithms to mitigate partial shading in building integrated PV system," *Solar Energy*, vol. 157, pp. 171-186, 2017/11/15/ 2017, doi: https://doi.org/10.1016/j.solener.2017.08.024.

[38] T. Guan and F. Zhuo, "An improved SA-PSO global maximum power point tracking method of photovoltaic system under partial shading conditions," in *2017 IEEE International Conference on Environment and Electrical Engineering and 2017 IEEE Industrial and Commercial Power Systems Europe (EEEIC / I&CPS Europe)*, 6-9 June 2017 2017, pp. 1-5, doi: 10.1109/EEEIC.2017.7977804.

[39] K. Sundareswaran, V. Vethanayagam, and S. P, "Application of a combined particle swarm optimization and perturb and observe method for MPPT in PV systems under partial shading conditions," *Renewable Energy*, vol. 75, 03/01 2015, doi: 10.1016/j.renene.2014.09.044.

[40] N. Kumar, I. Hussain, B. Singh, and B. K. Panigrahi, "Rapid MPPT for Uniformly and Partial Shaded PV System by Using JayaDE Algorithm in Highly Fluctuating Atmospheric Conditions," *IEEE Transactions on Industrial Informatics*, vol. 13, no. 5, pp. 2406-2416, 2017, doi: 10.1109/TII.2017.2700327.

[41] B. Sri Revathi and M. Prabhakar, "Non isolated high gain DC-DC converter topologies for PV applications – A comprehensive review," *Renewable and Sustainable Energy Reviews*, vol. 66, pp. 920-933, 2016/12/01/ 2016, doi: https://doi.org/10.1016/j.rser.2016.08.057.

[42] F. A. a. K. Eguchi, "Dynamics and Control of DC-DC Converters," 2018, ch. 1, pp. 1-2.

[43] S. Dahale, A. Das, N. Pindoriya, and S. Rajendran, *An overview of DC-DC converter topologies and controls in DC microgrid*. 2017, pp. 410-415.

[44] Z. Rehman, I. Al-Bahadly, and S. Mukhopadhyay, "Multiinput DC–DC converters in renewable energy applications – An overview," *Renewable and Sustainable Energy Reviews*, vol. 41, pp. 521-539, 2015/01/01/ 2015, doi: https://doi.org/10.1016/j.rser.2014.08.033.

[45] K. V. Raghavendra *et al.*, "A Comprehensive Review of DC–DC Converter Topologies and Modulation Strategies with Recent Advances in Solar Photovoltaic Systems," *Electronics*, vol. 9, no. 1, 2020, doi: 10.3390/electronics9010031.

[46] R. B. Darla, "Development of maximum power point tracker for PV panels using SEPIC converter," in *INTELEC 07 - 29th International Telecommunications Energy*

Conference, 30 Sept.-4 Oct. 2007 2007, pp. 650-655, doi: 10.1109/INTLEC.2007.4448860.

[47] D. G and S. N. Singh, "Selection of non-isolated DC-DC converters for solar photovoltaic system," *Renewable and Sustainable Energy Reviews*, vol. 76, pp. 1230-1247, 2017/09/01/ 2017, doi: https://doi.org/10.1016/j.rser.2017.03.130.

[48] R. Kumar. "Boost Converters – Working, Application & Advantages." EEWeb. https://www.eeweb.com/boost-converters-working-application-advantages/ (accessed 18th, April, 2021).

[49] "Modeling and Control of dc/dc Boost Converter in FC systems." http://www-personal.umich.edu/~annastef/FuelCellPdf/problemboostconverter.pdf (accessed.

[50] B. Hauke, "Basic Calculation of a Boost Converter's Power Stage," January 2014.

[51] B. Qinghai, "Analysis of Particle Swarm Optimization Algorithm," *Computer and Information Science*, vol. 3, 01/18 2010, doi: 10.5539/cis.v3n1p180.

[52] T. C. Havens, C. J. Spain, N. G. Salmon, and J. M. Keller, "Roach Infestation Optimization," in *2008 IEEE Swarm Intelligence Symposium*, 21-23 Sept. 2008 2008, pp. 1-7, doi: 10.1109/SIS.2008.4668317.